Summer 2010

Wavelet-Based Enhancement Technique for Visibility Improvement of Digital Images

Numan Ünaldı
Old Dominion University

WAVELET-BASED ENHANCEMENT TECHNIQUE FOR

VISIBILITY IMPROVEMENT OF DIGITAL IMAGES

by

Numan Ünaldı
B.S., June 1999, İstanbul Technical University
M.S., January 2005, Dokuz Eylül University

A Dissertation Submitted to the Faculty of
Old Dominion University in Partial Fulfillment of the
Requirements for the Degree of

DOCTOR OF PHILOSOPHY

ELECTRICAL AND COMPUTER ENGINEERING

OLD DOMINION UNIVERSITY
August 2010

Approved by:

Vijayan K. Asari (Director)

Zia-ur Rahman (Member)

Jiang Li (Member)

Norou Diawara (Member)

Okyay Kaynak (Member)

ABSTRACT

WAVELET-BASED ENHANCEMENT TECHNIQUE FOR VISIBILITY IMPROVEMENT OF DIGITAL IMAGES

Numan Ünaldı
Old Dominion University, 2010
Director: Dr Vijayan K. Asari

Image enhancement techniques for visibility improvement of color digital images based on wavelet transform domain are investigated in this dissertation research.

In this research, a novel, fast and robust wavelet-based dynamic range compression and local contrast enhancement (WDRC) algorithm to improve the visibility of digital images captured under non-uniform lighting conditions has been developed. A wavelet transform is mainly used for dimensionality reduction such that a dynamic range compression with local contrast enhancement algorithm is applied only to the approximation coefficients which are obtained by low-pass filtering and down-sampling the original intensity image. The normalized approximation coefficients are transformed using a hyperbolic sine curve and the contrast enhancement is realized by tuning the magnitude of the each coefficient with respect to surrounding coefficients. The transformed coefficients are then de-normalized to their original range. The detail coefficients are also modified to prevent edge deformation. The inverse wavelet transform is carried out resulting in a lower dynamic range and contrast enhanced intensity image. A color restoration process based on the relationship between spectral bands and the luminance of the original image is applied to convert the enhanced intensity image back to a color image. Although the colors of the enhanced images produced by the proposed algorithm are consistent with the colors of the original image, the proposed algorithm fails to produce color constant results for some "pathological" scenes that have very strong spectral characteristics in a single band. The linear color restoration process is the main reason for this drawback. Hence, a different approach is required for tackling the color constancy problem. The illuminant is modeled

having an effect on the image histogram as a linear shift and adjust the image histogram to discount the illuminant. The WDRC algorithm is then applied with a slight modification, i.e. instead of using a linear color restoration, a non-linear color restoration process employing the spectral context relationships of the original image is applied. The proposed technique solves the color constancy issue and the overall enhancement algorithm provides attractive results improving visibility even for scenes with near-zero visibility conditions.

In this research, a new wavelet-based image interpolation technique that can be used for improving the visibility of tiny features in an image is presented. In wavelet domain interpolation techniques, the input image is usually treated as the low-pass filtered subbands of an unknown wavelet-transformed high-resolution (HR) image, and then the unknown high-resolution image is produced by estimating the wavelet coefficients of the high-pass filtered subbands. The same approach is used to obtain an initial estimate of the high-resolution image by zero filling the high-pass filtered subbands. Detail coefficients are estimated via feeding this initial estimate to an undecimated wavelet transform (UWT). Taking an inverse transform after replacing the approximation coefficients of the UWT with initially estimated HR image, results in the final interpolated image.

Experimental results of the proposed algorithms proved their superiority over the state-of-the-art enhancement and interpolation techniques.

Keywords: Image enhancement, visibility improvement, wavelet domain enhancement, interpolation.

To my wife and my son,
I thank you for your endless love and support.

ACKNOWLEDGEMENTS

First of all, I would like to thank my advisor, Dr. Vijayan K. Asari for his constant support and guidance during my PhD study and dissertation research. His encouragement, patience, and concern allowed me to complete this study. My research was funded by Turkish Air Force of which I am very proud of being a member since 1997.

I would like to express my thanks to Dr. Zia-ur Rahman for being a member of my committee and for discussions on image and signal processing, from which I benefited greatly. I would also like to thank my dissertation committee members, Dr. Jiang Li, Dr. Norou Diawara and Dr. Okyay Kaynak for reviewing my dissertation.

I would like to thank all my friends and family members especially my parents-in-law for their support of my academic studies. I am grateful to my parents and my sister whose caring, understanding, and support helped me my whole life. Finally, I am thankful to my wife Dr. Nurdan Ünaldı for her unconditional support and love and to my son, Orhan, for letting me study instead of playing with him most(!) of the time.

TABLE OF CONTENTS

LIST OF FIGURES

LIST OF TABLES

Chapter I

INTRODUCTION

1.1 Motivation for the Dissertation Research

It is well known that human eyes perform much better than cameras when imaging real-world scenes, which generally have high dynamic range that can span more than six orders of magnitude. Human eyes have about 10^8:1 absolute range from fully adapted dark vision to fully adapted lighting conditions at noon on the equator. They can see about 3×10^4:1 range of luminance when adapted to a normal working range. This is achieved through a series of adaptive mechanisms for brightness perception. First, the size of pupil is variable to accommodate different levels of radiance from different regions in a scene while the camera aperture is fixed when capturing the scene. When staring at a highly-bright region in the scene, the pupil will shrink to compress the dynamic range so that the eyes can deal with it. Second, and more importantly, the major dynamic range compression process is taking place via the lateral processing at the retinal level [1]. Finally, the early visual cortex is also found participating in some of the dynamic range processing.

Conventional imaging devices, e.g. consumer cameras can measure only about three orders of magnitude. In addition, image display devices, like monitors and printers, also demonstrate limited dynamic range. As a result, images of high dynamic ranges scenes commonly suffer from poor visibility due to either overexposure causing saturation or underexposure resulting in low contrast dark images in which some important features are lost or become hard to detect by human eyes. Computer vision algorithms also have difficulty processing such images.

The Human Visual System (HVS) perceives the color of an object independent of the type of light illuminating it. A red apple illuminated by different light sources with

different spectral characteristics, still tends to appear red even though reflected spectrum is not same each time. Additionally, a yellow patch illuminated with white light or a white patch illuminated with yellow light reflect the same spectral distribution, but the yellow patch is seen as yellow and the white patch as white. This phenomenon is known as color constancy, e.g. the ability to remove the effect of the illumination from the output. The HVS has a complex non-linear mechanism of neuro-physiological functions of individual neurons that determines the perceived color discounting the illuminant through spatial and spectral comparisons of color signals across a scene.

Image enhancement is an important topic in digital image processing. It can help humans and computer vision algorithms obtain more accurate information from enhanced images. The visual quality and certain image properties, such as brightness, contrast, signal-to-noise ratio, resolution, edge sharpness, and color accuracy can be improved through the enhancement process. Many image enhancement algorithms have been developed based on various digital image processing techniques and applications. They can be developed in the spatial domain, spatial-frequency domain, or space-frequency domain (e.g., wavelet transform domain).

In many image processing applications, magnifying the details in an image may also be required, especially when the resolution is limited. Digital satellite, aerial images, and medical imaging along with distant object/face recognition are examples of such applications. It is necessary to make the magnification (interpolation) without blurring for the magnified details to be useful for object/face recognition.

Due to different properties of various image processing techniques employed in image enhancement algorithms, each algorithm may have certain specialties compared to other algorithms in terms of capability, performance, robustness, computation load, algorithm complexity, and so on. Therefore, it is necessary to investigate different image processing techniques to develop new image enhancement algorithms or to improve existing algorithms for the purpose of improving the visibility in scenes and strengthening the capability to deal with various image processing and computer vision applications.

This dissertation research is dedicated to developing an innovative image enhancement

technique for improving the visibility of low quality digital images caused by many reasons such as high dynamic range scene irradiance, poor contrast due to the very narrow dynamic range of the captured scene, very low illumination (low light conditions), pathological scenes that violate the gray-world assumption, non-uniform illumination or the spectral characteristics of the illuminant, and the limited resolution of the imaging devices. This research is focused into developing an algorithm that can automatically (without any human interventions) enhance images suffering from the previously mentioned effects.

1.2 Summary of the Dissertation Contributions

In this dissertation research, a novel, fast and robust wavelet-based dynamic range compression and local contrast enhancement (WDRC) algorithm to improve the visibility of digital images captured under non-uniform lighting conditions has been developed. Wavelet transform is used especially for dimension reduction such that the WDRC algorithm is applied only to the approximation coefficients which are obtained by low-pass filtering and down-sampling the original intensity image. The normalized approximation coefficients are transformed using a hyperbolic sine curve and the contrast enhancement is realized by tuning the magnitude of the each coefficient with respect to surrounding coefficients. The transformed coefficients are then de-normalized to their original range. The detail coefficients are also modified to prevent the edge deformation. The inverse wavelet transform is carried out resulting in a low dynamic range and contrast enhanced intensity image. A color restoration process based on the relationship between spectral bands and the luminance of the original image is applied to convert the enhanced intensity image back to a color image.

The proposed image enhancement algorithm, which provides dynamic range compression, while preserving the local contrast and tonal rendition, is also a good candidate for real time video processing applications. Although the colors of the enhanced images produced by the proposed algorithm are consistent with the colors of the original image, the proposed algorithm fails to produce color constant results for some

"pathological" scenes that have very strong spectral characteristics in a single band. The linear color restoration process is the main reason for this drawback. Hence, a different approach is required for tackling the color constancy problem. The illuminant is modeled having an effect on the image histogram as a linear shift and adjust the image histogram to discount the illuminant. The WDRC algorithm is then applied with a slight modification, i.e. instead of using a linear color restoration, a non-linear color restoration process employing the spectral context relationships of the original image is applied. The proposed technique solves the color constancy issue and the overall enhancement algorithm provides attractive results improving visibility even for scenes with near-zero visibility conditions. The scheme of the WDRC algorithm is shown in Figure 1.1.
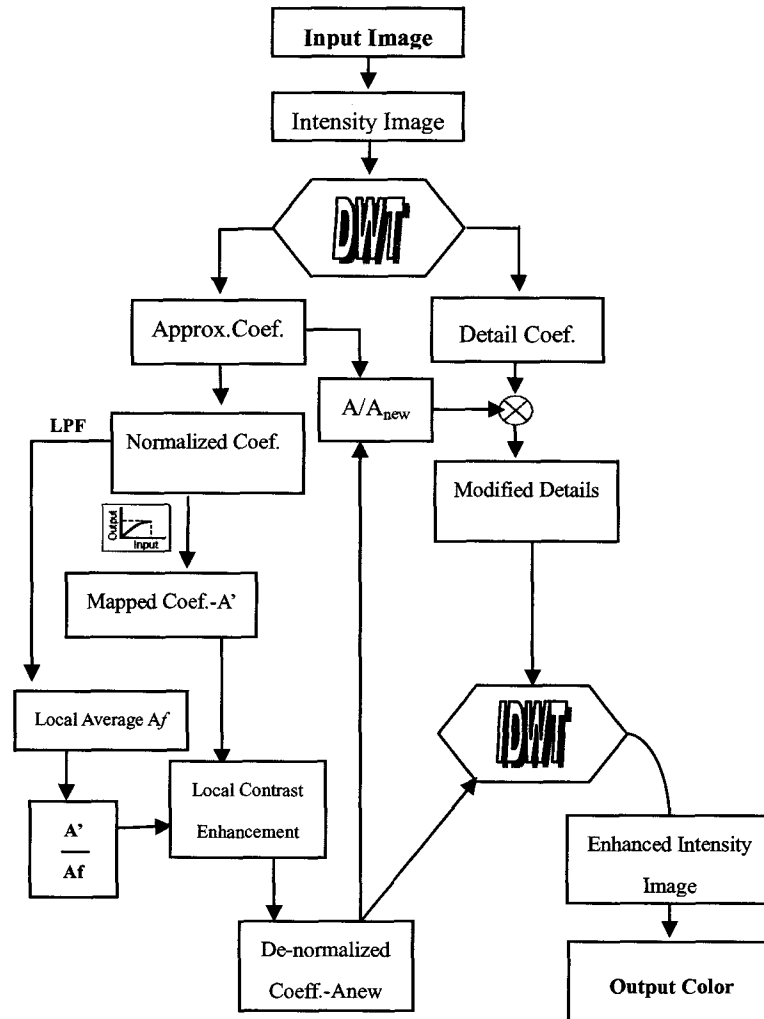
Figure 1.1 The proposed WDRC algorithm

In this research, new wavelet-based image interpolation technique that can be used for improving the visibility of tiny features in an image, is also presented. In wavelet domain interpolation techniques, the input image is usually treated as the low-pass filtered subbands of an unknown wavelet-transformed HR image, and then the unknown high-resolution image is produced by estimating the wavelet coefficients of the high-pass filtered subbands. The same approach is then used to obtain an initial estimate to the high-resolution image by zero filling the high-pass filtered subbands. Detail coefficients are then estimated via feeding this initial estimate to an undecimated wavelet transform (UWT). Taking an inverse transform after replacing the approximation coefficients of the UWT with initially estimated HR image, results in the final interpolated image.

Experimental results of the proposed algorithms proved their superiority over the state-of-the-art enhancement and interpolation techniques.

1.3 Specific Objectives

The specific objectives of this research are:

- Development of a nonlinear function which mimics the HVS for simultaneously enhancing the dark regions and compressing the bright regions in a high contrast image .

- Development of a context-dependent technique that is applied to the approximation coefficients of the discrete wavelet transform of the image that is to be enhanced.

- Application of a contrast enhancement algorithm to the enhanced approximation coefficients to improve the local contrast.

- Development of a technique for modification of detail coefficients to preserve the fine details and regularity of the edges in the image.

- Development of a histogram modification technique to account for the illumination spectral variations in the scene.

- Development of a non-linear color restoration technique based on the relationship between spectral bands and the luminance of the original image and the enhanced intensity image to obtain the enhanced color image.

- Development of a wavelet-based interpolation technique to increase the visibility of tiny features in an image.

- Combining the enhancement algorithm with the interpolation technique.

- Testing and evaluation of the performance of the proposed algorithms on various images captured in different scenes with diverse lighting conditions.

1.4 Organization of the Dissertation

The remaining chapters are organized as follows:

In Chapter II, a literature review of the nonlinear image enhancement techniques with an emphasis on Retinex-based methods is presented. Among those techniques, MSRCR [29]-[33], AINDANE [42], and IRME [43] algorithms which are used as benchmarks to the proposed enhancement algorithms are introduced. A review of image interpolation techniques especially the wavelet-based interpolation methods is also presented.

Chapter III presents the new wavelet-based image enhancement algorithm: wavelet-based dynamic range compression and local contrast enhancement (WDRC). For the algorithm, the details of nonlinear dynamic range compression through approximation coefficients obtained from the wavelet transformed intensity image, the local contrast enhancement based on local statistics of the approximation coefficients, detail coefficient modification, and a linear color restoration process are explained. The algorithm is discussed using various experimental results showing its capability of enhancing images of scenes with various illumination conditions. Drawbacks of the proposed algorithm in discounting the illuminant spectral variations for providing color constancy and in enhancing the images of some "pathological" scenes are also discussed.

In Chapter IV, a new color restoration (CR) process applied to WDRC processed images for tackling the color constancy problems is presented. The two steps for the nonlinear color restoration are described, namely, the global histogram adjustment before applying the WDRC algorithm and the final color restoration. Comparisons of the modified WDRC algorithm (WDRC-CR) with other advanced techniques are performed and discussed in terms of color constancy, visual quality, and computational complexity.

In Chapter V, a new wavelet transform-based algorithm for image interpolation is presented, which uses undecimated wavelet transform (UWT) for estimation of the missing high frequency components i.e. the detail coefficients. For explaining the algorithm in detail, an efficient implementation of the UWT using "á trous algorithm" is explained as a preliminary and the application of UWT to the image interpolation is then introduced. Experimental results from the proposed algorithm are presented. Some performance comparisons of the proposed algorithm are also shown with the state-of-the-art wavelet-based and spatial domain interpolation techniques along with the conventional ones in terms of quantitative similarity measures. Finally, some examples that are processed by both non-linear enhancement and wavelet interpolation algorithms are shown.

Finally, Chapter VI presents the major contributions of this dissertation work and some comments on related future work.

CHAPTER II

LITERATURE REVIEW

2.1 Spatial Domain Image Enhancement Techniques

To cope with the high dynamic range scenes given the limited dynamic ranges of cameras, monitors, and printers, various image processing techniques which compress or modify dynamic range have been developed. Some of those are global histogram modification techniques, such as gamma adjustment, logarithmic compression, and levels/curves methods. However, those conventional methods generally have very limited performance such that some features may be lost during the image processing, or some cannot be sufficiently enhanced. The resulting images suffer from degraded global and local contrast which is related with the visual quality and the fine features.

2.1.1 Histogram Equalization-Based Techniques

Among the contrast enhancement techniques, histogram equalization (HE) and its modified versions are commonly used for enhancement. Although HE works well for scenes that have uni-modal or weakly bi-modal histograms, its performance is poor for scenes with strongly bi-modal histograms. To make it work for multi-modal histograms, adaptive histogram equalization (AHE) was introduced [2]. In AHE which is also called localized or windowed HE, histogram equalization is performed locally within an adjustable size window. AHE provides local contrast enhancement and performs better than normal HE. However, AHE suffers from intensive noise enhancement in "flat" regions and "ring" artifacts at strong edges due to its strong contrast enhancement [3]. In contrast limiting AHE (CLAHE [4,5]), undesired noise amplification is reduced by selecting the clipping level of the histogram and controlling local contrast enhancement. Multi-scale AHE (MAHE) [6] is the most advanced variation of HE. Unlike traditional

single scale techniques, wavelet-based MAHE is capable of modifying/enhancing the image components adaptively based on their spatial-frequency properties. Those advanced HE variations generally have very strong contrast enhancement, which is especially useful in feature extraction applications like medical imaging for diagnosis. They are not commonly used in processing color images probably because their strong contrast enhancement may lead to excessive noise or artifacts and cause the image to look unnatural. Applying HE techniques to equalize each color channel separately by neglecting the inter-component correlation would lead to an incorrect result due to the vectorial nature of the data, i.e. each pixel is represented by a vector with three components and the three components are mutually correlated. Therefore, HE based techniques based on joint processing of the three channels have been developed for processing color images. Those techniques can be classified in two main groups.

In the first approach color data are processed in RGB space. The "3-D histogram equalization" method [7] consists of three-dimensional (3-D) histogram specification in the RGB cube, with the output histogram being uniform. In [8] "histogram explosion", a 3-D technique that exploits the full 3-D gamut is proposed. For each point in the RGB cube corresponding to an image color, a ray that starts from some central point, passes through that point and reaches to the surface of the RGB cube is defined. Then, all points within a threshold distance of the ray are projected onto the ray. In this way, a 1-D histogram along the ray is created and, equalized to determine the new color value for the original point. Through this technique, color points are almost uniformly spread in the color space. The "histogram decimation" technique [9,10] attempts to uniformly scatter the color points over the full 3-D gamut iteratively by shifting the color points in the current space so that their average becomes the geometric center of the space. This is followed by dividing the current color space into eight equally-sized subspaces which are set as the current space for the next iteration. This procedure is repeated until the sub-space reaches its minimum value. Thus, the color points are spread to occupy the full

range. All of these methods have issues with modifying color hues, which leads, in general, to results that look unnatural, since the HVS is extremely sensitive to shifts in hue.

The second approach for color HE is to perform equalization in color spaces other than RGB, [11]-[13] such as the Hue-Saturation-Intensity (HSI) space. This allows one to modify either only intensity component or both intensity and saturation components leaving the hue intact so that the issues concerning the shifts in hue of the above mentioned methods are solved. In [12], a method to jointly equalize intensity and saturation is presented, concluding that modification of saturation is not advised because of the unnatural results. In [14], an adaptive-neighborhood approach that performs its equalization only on the brightness component of the color image is presented. The method is designed to increase the number of intensity levels in the image by taking into account values of pixels within a certain neighborhood when computing the new intensity value of a pixel. The neighborhood is determined adaptively for each pixel in the image by a region growing algorithm, rather than forcing it to a predefined shape and size.

HE of the intensity component is only more effective in terms of computational cost and producing consistent colors that are not unnatural, compared to modifying the color channels separately. Nevertheless, all of the presented techniques are generally computationally expensive and have problems with either color consistency due to shifts in hue or color constancy (i.e. being independent from illuminant spectral distribution).

2.1.2   Retinex-Based Techniques

Land and McCann [15] carried out several experiments demonstrating that color perception is not just a simple signal acquisition. They concluded that perception in the HVS is realized by computations in the three retinal-cortical systems, each independently processing the low, middle, and high frequencies of the visible spectrum. They named

this process the Retinex (retina+cortex). In Retinex-based algorithms, the average of surface reflectance relative to the surrounding surface reflectance, so called lightness values, are computed in each of three distinct spectral bands for computation of the color of a pixel. This yields three distinct lightness values that give an invariant description of the surface-spectral-reflectance function at each wavelength, implying color constancy under some assumptions of image formation [22].

According to Land and McCann's original work [15] the lightness values of a pixel i in an image is determined by considering a certain number of paths, starting at random points and ending at i, and then by accumulating the logarithm of the ratios between the intensity values of subsequent points in the paths with the ratio is larger than a threshold. In the original work, the Retinex calculation consists of four steps, i.e. ratio, product, reset, and average [25]. With the exception of reset [21], these operators have remained the same since the introduction of the Retinex; only the way in which these operators are applied to the image changed. The main difference in several variants [16]-[21] of the original work is the way in which the comparisons of the pixel values with other pixels in the image are carried out. Thus, the computational complexity is improved while preserving the basic principles.

Through the years, the Retinex model has inspired a great variety of implementation and discussion, with results that are generally difficult to compare with each other [15]-[36]. Even Land and McCann presented different Retinex versions. In [21] Land presents the last version of his Retinex computation which has the following mathematical form:

$$R_{i\,out}(x,y) = \log I_i(x,y) - \log[F(x,y) * I_i(x,y)] \qquad (2.1)$$

where $I_i(x,y)$ is the image distribution in the i'th color spectral band, "$*$" denotes the convolution operation, $F(x,y)$ is the surround function, and $R_{i\,out}(x,y)$ is the associated retinex output with the i'th spectral band to produce Land's triplet values specifying color

and lightness. It is apparent that color constancy can be achieved with this form from (2.2)-(2.4):

$$I_i(x, y) = L_i(x, y)r_i(x, y) \tag{2.2}$$

where $L_i(x,y)$ is the spatial distribution of the source illumination and $r_i(x,y)$ is the distribution of scene reflectance. The reflectance component can be isolated if the illumination is known. Unfortunately, for arbitrary images the illumination is generally not known. However, if the intensity value at a pixel is divided by its spatially weighted average value, the following equation is obtained [22,28]:

$$R_{i_{out}}(x, y) = \log \frac{I_i(x, y)}{\overline{I_i}(x, y)} = \log \frac{L_i(x, y)r_i(x, y)}{\overline{L_i(x, y)r_i(x, y)}} \tag{2.3}$$

where the bars denote the spatially weighted average value. As long as $L_i(x, y) \approx \overline{L}_i(x, y)$ indicating the scene illumination is almost constant, then,

$$R_{i_{out}}(x, y) \approx \log \frac{r_i(x, y)}{\overline{r}_i(x, y)} \tag{2.4}$$

The approximate relation in (2.4) is equality for many cases and, for those cases where it is not strictly true, the reflectance ratio should dominate illumination variations [28].

Experiments conducted by Jobson *et al.* [28] show that Land's center/surround retinex achieves color constancy and dynamic range compression; but not a good visual rendition. Specifically, halo artifacts appear where uniform regions come together to form a high contrast edge "graying" in the large uniform zones in an image. Besides, global violations of the gray world assumption (e.g., scenes that are dominated by one color) cause a global "graying out" of the image. In [28], they investigated the properties of "Centre/Surround Retinex" and suggested solutions to some implementation issues they encountered during their experimental investigations of the algorithm. Their implementation, later so called Single Scale Retinex (SSR) aims to produce color constant and dynamic range compressed images with satisfactory rendition. To fulfill this,

it specifies the placement of the log function; the functional form of the surround; the space constant for the surround; and the treatment of the retinex triplets prior to display. To summarize the characteristics of the SSR algorithm [28]:

1. The functional form of the surround is a Gaussian.

2. The placement of the log function is AFTER surround formation.

3. The post-retinex signal processing is a "canonical" gain/offset rather than an automatic gain/offset.

4. There is a trade-off between dynamic range compression and tonal rendition which is governed by the Gaussian surround space constant.

5. A single scale is incapable of simultaneously providing sufficient dynamic range compression and tonal rendition

6. Violations of the gray-world assumption lead to retinexed images which are either "grayed-out" locally or globally or, more rarely, suffered from color distortion.

Since the width of the surround affects the rendition of the processed image, multiple scale surrounds were found to be necessary to provide a visually acceptable balance between dynamic range compression and graceful tonal rendition.

The Multiscale Retinex (MSR) [29]-[33] combines the dynamic range compression of the small scale retinex with the tonal rendition of the large scale retinex to produce an output which encompasses both. The equations for the MSR are defined by

$$R_i(x,y) = G_r \sum_{k=1}^{K} W_k \{\log I_i(x,y) - \log[F_k(x,y) * I_i(x,y)]\} - O_r,$$

$$i = 1, \cdots, N$$

(2.5)

where the subscripts i represents i'th spectral band and N is the number of the spectral bands: $N=1$ for grayscale images and $N=3$, $i \in \{R,G,B\}$ for typical color images. K is the number of scales used in computations (with $K=1$ the equation turns to be SSR) and

W_k are the weighting factors for the scales, G_r and O_r are the gain and offset values that map the result of the retinex computation from retinex domain to display domain.

Although the number of scales used for the MSR is application-dependent, it was empirically found that a combination of three scales representing narrow, medium, and wide surrounds is sufficient to provide both dynamic range compression and tonal rendition [29]-[33]. The narrow-surround acts as a high-pass filter, capturing all the fine details in the image but at a severe loss of tonal information. The wide-surround captures all the fine tonal information but at the cost of dynamic range. The medium surround captures both dynamic range and tonal information. The MSR is the average of the three renditions [33].

The halo artifacts around uniform regions that come together to form a high contrast edge caused by a small scale also lessen when multiple scales are used. The MSR still suffers from graying out of uniform zones much as the SSR does. This occurs because the retinex processing enhances each color band separately. The smaller values in the weaker channels get "pushed" up strongly, making them approximately equal in magnitude to the dominant channel, leading to a graying out of the overall region, which, in some cases, is severe. Unexpected color distortions in rare occasions are also reported due to gray-world violations [33]. Therefore, a color restoration scheme to remove this drawback is considered. MSR with color restoration (MSRCR) is mathematically represented as:

$$R_{MSRCR_i} = \alpha_i(x, y) \cdot R_{MSR_i}(x, y) \tag{2.6}$$

with

$$\alpha_i(x, y) = \beta \log \left[I_i(x, y) \bigg/ \sum_{i=1}^{N} I_i(x_1, x_2) \right] + \gamma \tag{2.7}$$

where β and γ are the color gain and color offset values, respectively. Again a single set of values for β and γ was determined for all spectral channels. There is an analogy between the internal forms of the retinex process and the color restoration process. Both

computations are contextual, highly relative, and nonlinear. The MSRCR provides the necessary color restoration, eliminating the color distortions and gray zones evident in the MSR output. However, MSRCR does not completely restore the bright colors that are in the original image. To handle that, a white balance [33] process is applied. The pixel intensities of the original image and the MSRCR output are compared, and maximum of either one is accepted for each pixels.

Although MSRCR performs well for a very large variety of natural images, processing in three spectral channels for at least three scales makes the algorithm hard to implement for real-time applications on contemporary PC platforms. In addition, optimal performance is not always obtained with default parameter setting, especially when images that have a dark subject with a very bright background are being processed, MSRCR seems to have difficulty providing sufficient luminance enhancement for the subject. Besides, MSRCR with default parameters cannot handle the images with a very narrow dynamic range, such as images taken under turbid imaging condition without post-enhancement treatment. Moreover, there is a trade-off between using white-balance or not in MSRCR processing. If white-balance is turned-off, the uniform bright regions in the original image turn to gray in the enhanced image, but local contrast is improved even for the brightest regions. When white-balance is turned on this drawback is overcome, however, the enhancement of only dark regions can be achieved. Actually, the former is useful for computer vision applications, whereas the latter produces good rendition. Finally, the "halo effect" appearing at the boundaries with a large luminance change between the large uniform regions even though reduced, is not totally removed.

In a more recent work [37], to overcome all the drawbacks addressed in the previous paragraph, Jobson *et al.* have developed their method with a fundamental shift in approach away from purely passive retinex processing to an active measurement and control system. The so called Visual Servo (VS) concept is shown in Figure 2.1. In VS enhancement, a key visual parameter is first measured, second, based upon the measured value, an enhancement control to improve the overall brightness, contrast, and sharpness of the image is activated followed by recomputing the visual measure. If the measured

value of the parameter achieves a predefined visual standard based upon the local image statistics, then the process is terminated; otherwise, the process is iterated until either the visual standard has been achieved or the VS has determined internally that all reasonable enhancement processing has been exhausted.
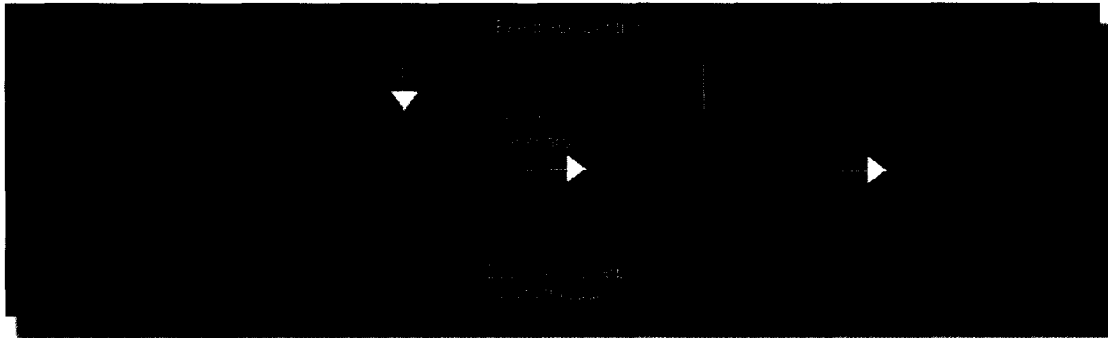
Figure 2.1 The Visual Servo Enhancement (courtesy of NASA).

A bunch of VS-processed image examples can be seen on the related internet site [38]. Those demonstrations show that visual servo automatically matches the type and degree of image enhancement to the type and degree of visual deficit in raw image data. The only drawback of this kind of enhancement is that it is computationally more extensive with its iterative nature than the passive form.

Inspired by the MSRCR enhancement, many other image enhancement techniques have been developed performing their computations on only the intensity channel following a linear color restoration process to produce the enhanced color images. Among those, Multi-scale Luminance Retinex [39] method is proposed to apply the MSRCR on only the luminance channel. Luma-Dependent Nonlinear Enhancement (LDNE) [40,41] algorithm is another luminance-based multi-scale center/surround retinex algorithm. Adaptive Integrated Neighborhood Dependent Approach for Nonlinear Enhancement (AINDANE) [42] and Illuminance-Reflectance Model for Nonlinear Enhancement (IRME) [43] both implement adaptive luminance enhancement and adaptive contrast enhancement separately. Multi-Windowed Inverse Sigmoid (MWIS) [44] is an extension of IRME, replacing the inverse sigmoid function used in IRME for

adaptive luminance enhancement, by two combined sigmoid functions to deal with the bright regions as well. Locally Tuned Sine Nonlinearity (LTSN) is another extension of [45] utilizing the trigonometric function for illuminance enhancement to achieve the enhancement of dark and bright regions simultaneously. These techniques differ from each other in the way they perform luminance enhancement. In all these methods, the enhanced chromatic image component is obtained by using a linear color restoration process based on the chromatic information in the original image. Although these algorithms provide dynamic range compression to some extent, it is not possible to achieve color constancy by just modifying the luminance channel, since the chromatics of the original image are used linearly to restore the color, which stands in direct contrast to the color constancy objectives of the Retinex. The proposed enhancement algorithm in this dissertation is based on AINDANE and IRME in some aspects, therefore these two techniques are briefly introduced for completeness of the dissertation report.

2.1.2.1 AINDANE

The AINDANE algorithm [42] consists of two parts: adaptive luminance enhancement and adaptive contrast enhancement. The luminance enhancement part is an intensity transformation with a nonlinear transfer function. The contrast enhancement part, which is adaptively controlled by the global statistics of the image, tunes the intensity of each pixel based on its relative magnitude with respect to the neighboring pixels. To convert color images to intensity (gray-scale) images, the National Television System Committee (NTSC) standard is used, which is defined as:

$$I(x,y) = \frac{76.245R + 149.6851G + 29.07B}{255} \tag{2.8}$$

where R,G and B are the values of the red, green and blue color band of a pixel. Then the image intensity is normalized as:

$$I_n(x,y) = \frac{I(x,y)}{255} \tag{2.9}$$

followed by the nonlinear mapping by the transfer function given by (2.10) to get dynamic range compression.

$$I_n{}'(x,y) = \frac{I_n(x,y)^{(0.75z+0.25)} + 0.4(1 - I_n(x,y))(1 - z) + I_n(x,y)^{(2-z)}}{2} \tag{2.10}$$

where z provides the curve of the transfer function and is related to the image histogram defined as:

$$z = \begin{cases} 0 & for & L \le 50 \\ \dfrac{L-50}{100} & for & 50 < L \le 150 \\ 1 & for & L > 150 \end{cases} \tag{2.11}$$

where L is the intensity level corresponding to where the cumulative gray level distribution is 0.1. L is used as an indication to determine how dark the lowest 10% of pixels in an image are. If the z value is 0, the pixel will be a maximum enhanced level and if the z value is 1, no pixel will be enhanced.

A surrounding pixel (neighborhood) dependent contrast enhancement method is implemented to achieve sufficient contrast for image enhancement. The luminance information of surrounding pixels is obtained by using 2D discrete spatial convolution with a Gaussian kernel. The center-surround contrast enhancement $S(x, y)$ is carried out as defined in the following equation:

$$S(x,y) = 255 I_n{}'(x,y)^{E(x,y)} \tag{2.12}$$

where $E(x,y)$ is the inverse of the center-surround ratio raised with a parameter P.

$$E(x,y) = \left[\frac{I_{conv}(x,y)}{I(x,y)} \right]^P \tag{2.13}$$

where the parameter P is related to the global standard deviation of the input intensity

image, $I(x, y)$, and can be determined as:

$$P = \begin{cases} 3 & for & \sigma \leq 3 \\ \dfrac{27 - 2\sigma}{7} & for & 3 < \sigma < 10 \\ 1 & for & \sigma \geq 10 \end{cases} \qquad (2.14)$$

where global standard deviation σ is the indication of the contrast level of the original intensity image. If the contrast of original image is poor, P will be larger and further increase the contrast enhancement.

The contrast enhancement defined by (2.12) is carried out for the surround formations via three different scaled convolutions and the results are averaged as in MSR to get the enhanced intensity image. Finally, the enhanced color image can be obtained by linear color restoration based on chromatic information contained in the original image as:

$$S_j(x, y) = S(x, y) \frac{I_j(x, y)}{I(x, y)} \lambda_j \qquad (2.15)$$

where j represents the RGB spectral band and λ_j are parameters which adjust the color hue.

2.1.2.2 IRME

IRME [43] is an image enhancement algorithm based on a physical description of the creation of a radiance map of the real world scene. It divides the object radiance into two parts: illumination and reflectance. IRME runs its computations on the illumination and leaves the reflectance unchanged to improve the visual perception of those scenes.

The algorithm consists of four steps: (a) illumination estimation and reflectance extraction; (b) adaptive dynamic range compression of illuminance; (c) adaptive mid-tone frequency components enhancement; (d) image restoration.

The first step of the algorithm is to obtain the intensity image, i.e. the value component of the HSV color space. Based on the relation given in (2.2), reflectance is

extracted. Following the assumption that the illumination $L(x, y)$ is slowly varying it is assumed to be contained in the low frequency components of the image and a Gaussian low-pass filtered result of the intensity image is used in estimating the illumination. This process is realized by using a 2-D discrete spatial convolution of the intensity image with a Gaussian kernel of a narrow surround, i.e. 2~5.

In the second step, adaptive dynamic range compression of illuminance is performed using the windowed-inverse sigmoid (WIS) function. The sigmoid function is defined as:

$$f(v) = \frac{1}{1 + e^{-av}} \tag{2.16}$$

where a is a parameter that determines the steepness of the curve shape. This function is used as the intensity transfer function for dynamic range compression by performing the equations (2.17)-(2.19).

$$L_n' = L_n[f(v_{max}) - f(v_{min})] + f(v_{min}) \tag{2.17}$$

$$L_n'' = \frac{1}{a} \ln\left(\frac{1}{L_n'} - 1\right) \tag{2.18}$$

$$L_{n,enh} = \frac{L_n'' - v_{min}}{v_{max} - v_{min}} \tag{2.19}$$

where Equation (2.17) linearly maps the input range [0,1] of the normalized illuminance L_n to the range $[f(v_{min}), f(v_{max})]$ to be an input to the windowed-inverse sigmoid. Equation (2.18) is the inverse sigmoid function. Equation (2.19) is applied to normalize the output illuminance L_n'' to range [0,1]. Parameters v_{max} and v_{min} are used to tune the curve shape of the transfer function. The coefficient v_{min} is empirically determined by the global mean I_m of the intensity image as:

$$v_{min} = \begin{cases} -6 & \text{for } I_m \leq 70 \\ 3\left(\frac{I_m - 230}{80}\right) & \text{for } 70 < I_m < 150 \\ -3 & \text{for } I_m \geq 150 \end{cases} \tag{2.20}$$

The third step of the IRME is adaptive mid-tone frequency component enhancement which is same as the contrast enhancement part of AINDANE for a single medium scale of the Gaussian. The enhanced intensity image is obtained by multiplying the modified illumination $L'_{n,enh}(x, y)$ and reflectance $R(x, y)$ and is expressed as:

$$I'(x, y) = L'_{n,enh}(x, y)R(x, y) \tag{2.21}$$

Color restoration in IRME is also same as AINDANE's with λ_j in (2.15) are taken as unity in IRME.

2.2 Wavelet Transform Domain Image Enhancement Techniques

Mathematical formulation of signal expansion using wavelets gives wavelet transform (WT) pairs, which is analogous to the Fourier transform (FT), in which signals are represented as a sum of sinusoids. A 'wavelet' is a small wave which has its energy concentrated in time with varying frequency and limited duration. The WT has the ability to provide both spatial (or temporal) and frequency information (i.e. space-frequency or time-frequency analysis) thus it is a suitable tool for transient, non-stationary or time varying phenomena whereas the non-local FT gives only frequency information. The need for simultaneous representation and localization of both time and frequency for non-stationary signals (e.g. speech and music) led toward the evolution of WT from the popular FT. The WT has been investigated and applied to many image processing problems.

Based on several fields, i.e. subband coding from signal processing [46], quadrature mirror filtering (QMF) from speech recognition [47], and pyramidal image processing [48], Mallat [49] first proposed multiresolution analysis (MRA) by using the WT. This turned to be a powerful signal processing tool resulting in a very wide area of applications including image denoising [50]-[52], image coding or compression [53],

image enhancement [54]-[56], detection and classification [57], and synthesis [58]. Most importantly, the WT has been adopted in the state-of-art image and video compression standards like JPEG-2000 and MPEG-4 [59, 60].

2.2.1 Wavelet-based Image Enhancement Techniques

Wavelet-based image enhancement is mainly used to enhance the perceptual quality of an image. Due to its band-pass nature, through which edges in an image can be located, the WT is well suited for improving the edge features in an images. By appropriately modifying edges, sharpness, and the local contrast can be enhanced leading to improved visual quality.

Multi-scale image contrast enhancement has been proposed and implemented using either wavelets, especially in medical imaging application [56]-[60], or curvelet [55] transform for color and gray scale image enhancement. Velde [56] proposes modifying the wavelet coefficients in a contrary way to the coefficient thresholding in wavelet denoising algorithms, strengthening the weakest edges (small valued coefficients) and leaving the strongest edge unmodified. In [55], Velde's approach is realized in a curvelet domain with a slight modification to the mapping function applied for modifying the wavelet coefficients.

Fu *et al.* [58] analyzing Histogram Equalization (HEQ) in the spatial domain, propose a method in wavelet domain to achieve contrast enhancement. They first perform the HEQ in the spatial domain and then perform the WT on the equalized image. Then, all approximation-coefficients are squared. They claim that this process compensates for the information that was lost during the HEQ process. Reeves *et al.* [59] investigate a WT domain filter based on locally adaptive linear minimum mean squared-error (LLMMSE) filter to suppress noise and enhance edges. They also apply global HEQ to the image represented by the normalized approximation coefficients at the coarsest decomposition level. Peng *et al.* [60] propose an approach using shift invariant wavelet transform for the contrast enhancement of radiographs. The edge information of radiographic images is extracted and protected by exploiting cross-scale correlation among wavelet coefficients,

while noise is smoothed out in the wavelet domain. Radiographs are then reconstructed from the transform coefficients modified at multi-scales by nonlinear enhancement operator. Qin and El Sakka [61] propose a wavelet-based method for contrast/edge enhancement. The proposed method histogram equalizes the image represented by the normalized approximation-coefficients, while high-boost filtering the detail-coefficients at selected resolution levels separately to achieve robust contrast and edge enhancement.

In [62], a method to improve the perceptual quality of wavelet compressed images has been proposed. They model edges using the edge model of [63]. Edge parameters are modified in order to approach them to the ideal edge model. Edges are then reconstructed. Since the ideal edge model is not natural, neither are the algorithm results.

2.2.2   Wavelet-based Image Interpolation Techniques

Conventional techniques such as spline interpolation, nearest neighbor interpolation, bilinear interpolation, cubic convolution, b-spline, and tapered sinc [64]-[67] utilize the coherence of adjacent points. Although these techniques have advantages in simplicity and fast implementation, the result of these interpolations may degrade fine details in an image.

Linear interpolation tries to fit a straight line between two points. This technique leads to blurred image. Pixel replication copies neighboring pixel to the empty location. This technique tends to produce *blocky* images. Approaches like spline and sinc interpolation are proposed to reduce these two extremities. Spline interpolation is inherently a smoothing operation, while sinc produces ripples (the Gibbs phenomenon) in the output image.

The HVS is highly sensitive to edges, which play a key role in the perception of an image as high quality. Therefore, a good interpolation algorithm possesses a requirement to correctly reconstruct the original scene edges or at least maintain the sharp edges in the scene. Recently, nonlinear interpolation techniques [68]-[74] have been developed to

fulfill this requirement.

Wavelet-based interpolation techniques have been widely used for performing image interpolation for more than a decade. The input image is usually treated as the low-pass filtered subbands of an unknown wavelet-transformed high-resolution image, and then the unknown high-resolution image is produced by estimating the wavelet coefficients of the high-pass filtered subbands. The simplest approach is padding of the unknown high-pass filtered (detail) subbands with zeros and then taking the inverse wavelet transform. It is interesting to note that while this approach is capable of outperforming bilinear interpolation, it has never appeared in the literature probably due to its simplicity [75]. Nevertheless, various complex techniques have been presented to estimate the unknown HF wavelet coefficients to improve the quality of the reconstructed images.

Chang *et al.* [76] extrapolate the features in textured regions by examining the evolution of wavelet transform extrema and important singularities. Large magnitude coefficients are selected, since modeling for other coefficients is not easy. A least squares error criterion based approach is adopted to determine the corresponding extrema at the finest scale. Carey *et al.* [77] based on the same approach in [76], use the Lipschitz property, which states the wavelet coefficients corresponding to large singularities decay exponentially over scale [78]. At each index, an exponential fit over scale was used for wavelet coefficients to predict the detail coefficients at the finer scale. In both methods, only coefficients with large magnitude are used indicating moderate details cannot be treated this way. Moreover since the wavelet coefficients are formed by contributions from more than one coefficient in a neighborhood determined by the support of the filters used in the analysis, edge reforming based on extrema evolution that takes account of only significant magnitudes, affect the quality of edge reconstruction. Finally, signs of estimated coefficients are replicated directly from 'parent' coefficients without any attempt made to estimate the actual signs, implying that signs of the coefficients

estimated using extrema evolution techniques cannot be relied upon.

Crouse *et al.* [79] propose the use of the Hidden Markov Model (HMM) for predicting wavelet coefficients over scales. In the training phase, HMM is trained using an image database. They predict the *exact* coefficient from the *observed* coefficient of a noisy image, for denoising application. The principle used here is that the coarser scale coefficients are less affected by noise, while the detail coefficients contain most of the noise. The same idea is extended to image zooming by Kinebuchi and Woo [54]. They first use a hidden Markov tree model (HMT) to infer the probability of each hidden state and corresponding variances. Then, a Gaussian mixture model (GMM) (corresponding to the hidden states) is used for each wavelet coefficient and the wavelet coefficients in the highest subband are generated randomly (by sampling) using the estimated state probabilities and variances. In estimating variances, the property of exponential decay of variances was assumed [77] with roughly estimated exponents.

Greenspan *et al.* [80] and Burt *et al.* [81] both utilize the inter-scale dependency (mainly related to edges) to extrapolate lost high-frequency components and use zero-crossings of the second derivative of smoothed images to locate edges. Based on the ideal step edge model, they estimate the interscale relations of edges in order to estimate edges at finer scales.

Interpolation of interlaced sampling structure of the multiple low resolution (LR) images utilizing the multiresolutional basis fitting reconstruction (MBFR) technique [84], is applied to the wavelet based superresolution problem in [82] and [83]. In [85], MBFR is applied to a single LR image. Single LR interpolation does not give satisfactory results since a single LR image possesses uniform sampling, which does not suit MBFR.

The decimated WT is not shift-invariant and, as a result, suppression of wavelet coefficients, such as quantization of coefficients during the compression process or non-exact estimation of high-frequency subband coefficients, introduces cyclostationarity into the image which manifests itself as ringing in the neighborhood of discontinuities

[75]. Temizel and Vlachos [75] propose a method in which initially estimated HR image via zero padding is shifted and wavelet transformed several times with different amount of shifts each time, followed by the inverse wavelet transform and the shift back to their original location. The results from each shift-transform cycle is then averaged in order to remove the ringing artifacts appeared before cycle-spinning process.

Celik and Kusetogullari [86] present an interpolation technique using dual-tree complex wavelet transform (DT-CWT) [87,88] which exhibits approximate shift invariant property and improved directional resolution when compared that of the DWT. They estimate HR coefficients using different types of deformations obtained by bilateral filtering of the initially estimated HR image with different parameters followed by transforming each deformed HR image results, and the resultant HR image is computed by averaging the different reconstructions from LR image using different detail wavelet coefficient sets. The perceptual and objective quality of resolution enhanced images outperforms most recently proposed methods in the field.

CHAPTER III

WAVELET-BASED DYNAMIC RANGE COMPRESSION AND LOCAL CONTRAST ENHANCEMENT

3.1 Introduction

In this chapter, a new wavelet-based image enhancement algorithm to improve the visibility of low quality digital images is introduced. To achieve this aim, the algorithm provides dynamic range compression, local contrast enhancement, and color constancy simultaneously.

The proposed enhancement algorithm consists of four main stages, three of which are applied in discrete wavelet domain:

1. Luminance enhancement via dynamic range compression of approximation coefficients.

2. Local contrast enhancement using averaged luminance information of neighboring pixels which is inherited to approximation coefficients

3. Detail coefficients modification.

4. Color restoration.

The derivation of the algorithm will be introduced in detail and experimental results will be shown in the following sections. Comparisons of the proposed WDRC algorithm with other state-of-art techniques will be provided in Chapter 4 after introducing the new non-linear color restoration approach.

3.2 Dynamic Range Compression

For input color images, the intensity image $I(x,y)$ can be obtained with the following equation:

$$I(x,y) = \max[I_i(x,y)], \quad i \in \{R,G,B\} \tag{3.1}$$

This is the definition of the value (V) component in HSV color space. The enhancement algorithm is applied on this intensity image. According to 2D discrete wavelet transform, the luminance values are decomposed by (3.2):

$$
\begin{aligned}
I(x,y) = & \sum_{k,l \in z} a_{J,k,l} \Phi_{J,k,l}(x,y) + \sum_{j \geq J} \sum_{k,l \in z} d^h{}_{j,k,l} \Psi^h{}_{j,k,l}(x,y) \\
& + \sum_{j \geq J} \sum_{k,l \in z} d^v{}_{j,k,l} \Psi^v{}_{j,k,l}(x,y) + \sum_{j \geq J} \sum_{k,l \in z} d^d{}_{j,k,l} \Psi^d{}_{j,k,l}(x,y)
\end{aligned} \tag{3.2}
$$

where $a_{J,k,l}$ are the approximation coefficients at scale J with corresponding scaling functions $\Phi_{J,k,l}(x,y)$, and $d_{j,k,l} = (d^h, d^v, d^d)$ are the detail coefficients at each scale with corresponding wavelet functions $\Psi_{j,k,l}(x,y)$. While the first term on the right-hand side of (3.2) represents the coarse-scale approximation to $I(x,y)$, the second, the third, and the fourth terms represent the detail components in horizontal, vertical and diagonal directions, respectively.

Based on some assumptions about image formation and human vision behavior, the image intensity $I(x, y)$ can be simplified as a product of the reflectance $R(x, y)$ and the illuminance $L(x, y)$ at each point (x, y). The illuminance L is assumed to contain the low frequency component of the image while the reflectance R mainly includes the high frequency component, since R generally varies much faster than L does in most parts of an image with a few exceptions, like shadow boundaries. In most cases, the illuminance has dynamic range that is several orders larger when compared to reflectance. By compressing only the dynamic range of the illuminance and preserving the reflectance, dynamic range compression of the image can be achieved [43]. Estimation of illuminance of a scene from

an image is a difficult task. Many techniques have been developed to deal with this problem [20,24]. Low pass filtered result of the intensity image can be used for this purpose [43].

The WT, with which any image can be expanded as a sum of its approximate image at some scale J along with corresponding detail components at scale J and at finer scales, is used especially for dimension reduction in the algorithm. Additionally, the approximate image represented by normalized approximation coefficients is used, which can be obtained by low pass filtering and down-sampling the original image in the wavelet transform, to estimate the down-sampled version of the illuminance.

A raised hyperbolic sine function given in (3.3) which maps $a_{J,k,l}$ from range [0,1] to [0,1] is used for compressing the dynamic range represented by the coefficients. A hyperbolic sine function for dynamic range compression was chosen since the function is 'two-sided' that allows for pull-up of small coefficients and pull-down of large coefficients to some extent at the same time. This is consistent with the human visual system that has mechanisms through which it can adapt itself allowing good visual discriminat ion in all lighting conditions. The normalized and compressed coefficients at level J can be obtained by:

$$\overline{a}_{J,k,l} = \left[\frac{\sinh(4.6248a'_{J,k,l} - 2.3124) + 5}{10} \right]^{r} \tag{3.3}$$

where $a'_{J,k,l}$ are normalized coefficients given by (3.4) and r is the curvature parameter which adjusts the shape of the hyperbolic sine function.

$$a'_{J,k,l} = \frac{a_{J,k,l} - \min(a_{J,k,l})}{\max(a_{J,k,l}) - \min(a_{J,k,l})} \tag{3.4}$$

In Figure 3.1 the hyperbolic sine function with different curvature parameters is shown. To ease the comparison, identity transformation ($\overline{a}_{J,k,l} = a'_{J,k,l}$) is also given. For values of r

less than 1, small pixel values are pulled up much more than large pixel values are pulled down, and for values greater than 1, it is reversed. The default value of $r=0.5$ was determined which provides good range compression especially in shadowed scenes. Larger values of r were determined to be useful for bright scenes with no dark regions and for scientific applications such as medical image enhancement especially when the region of interest is too bright.
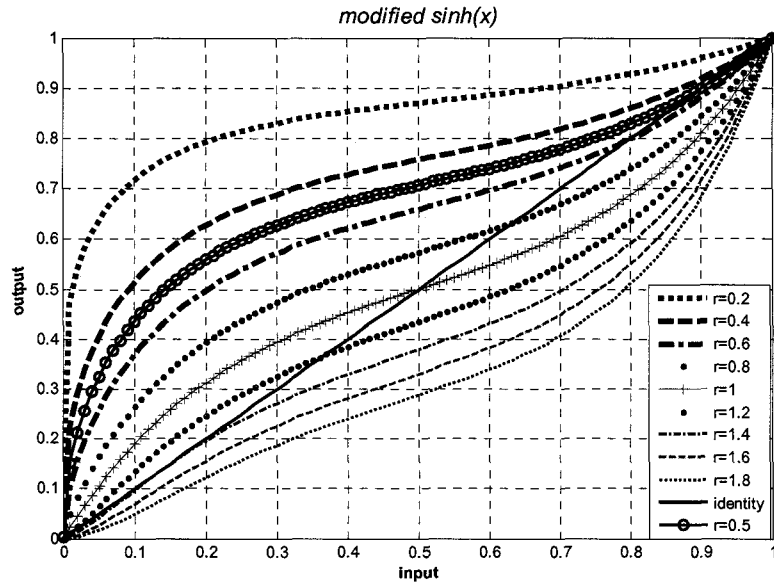
Figure 3.1 Modified hyperbolic sine function

After applying the mapping operator to the coefficients, if the new coefficients are de-normalized and the inverse wavelet transform is taken, the result will show a compressed dynamic range with a significant loss of contrast. The new image will look washed-out. Such an example is shown in Figure 3.2(b). Thus, the local contrast needs to be increased to improve the visual quality.

3.3 Local Contrast Enhancement

The global contrast enhancement techniques which modify the histogram of the image by stretching it or boosting the bright pixels and decreasing the value of dark

pixels globally, can not generally produce satisfying results. Those methods have limited performance in enhancing fine details especially when there are small luminance differences between adjacent pixels. Therefore, the surrounding pixels should be taken into account when one pixel is being processed. The "centre/surround ratio" introduced by Land [18], and efficiently modified by Jobson *et al.*[28] was used to achieve the compressed dynamic range preserving or even enhancing the local contrast.

The center/surround ratio is used as a variable gain matrix, by simply multiplying with the modified coefficients when the ratio is less than 1 and by applying inverse of this matrix as a power transform to the coefficients when the ratio is greater than 1. In such a

(a)   (b)
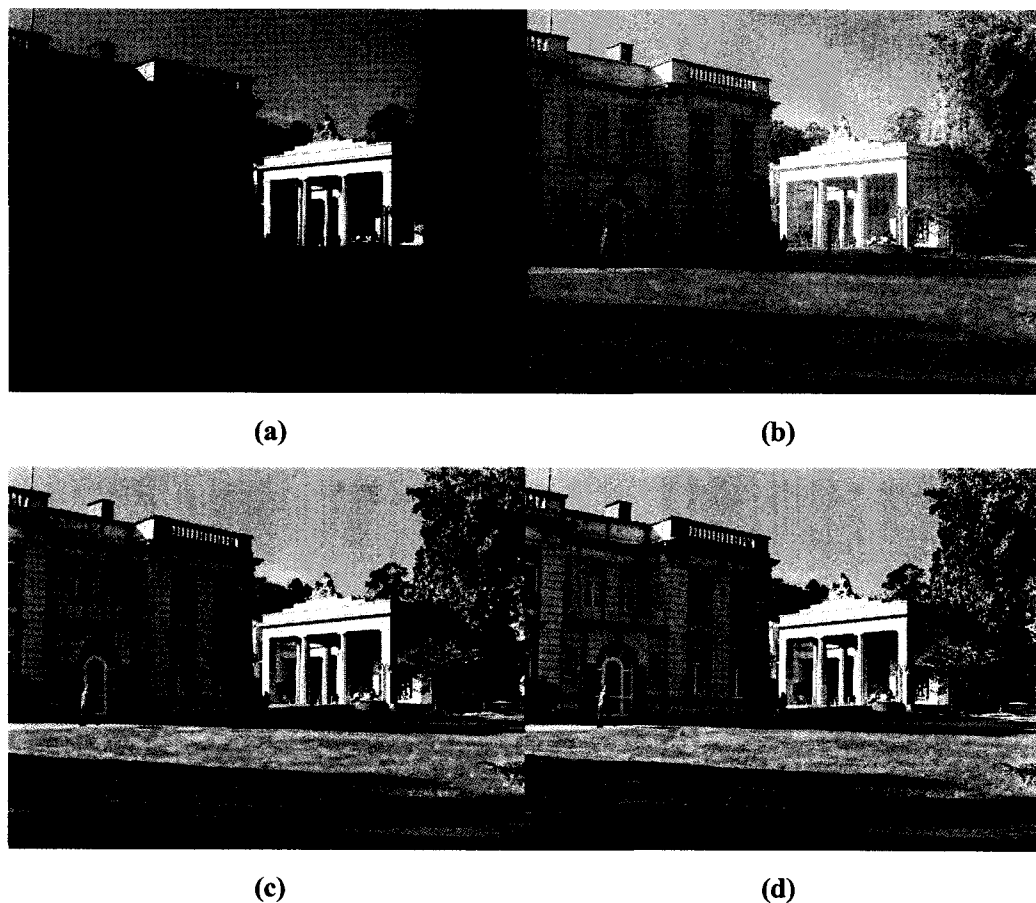
(c)   (d)

Figure 3.2 Results of the proposed algorithm at each step. (a) Original image; (b) Range compressed image; (c) Local contrast enhanced image; (d) Image with modified detail coefficients.

way, the processed images will not suffer either halo artifacts, or saturation caused by over-enhancement. In this technique, depending on their surrounding pixel intensity, pixels with the same luminance can have different outputs. When surrounded by darker or brighter pixels, the luminance of the pixel being processed (the center pixel) will be boosted or lowered respectively. As a result, image contrast and fine details can be sufficiently enhanced while dynamic range expansion can be controlled without degrading image quality.

The local average image represented by modified approximation coefficients is obtained by filtering the normalized coefficients obtained from the wavelet decomposition of the original image with a Gaussian kernel. A Gaussian kernel was chosen, like in MSRCR, which proved to give good results over a wide range of space constants. The standard deviation (also called scale or space constant) of the 2D Gaussian distribution determines the size of the surround. The 2D Gaussian function $G(x,y)$ is given by:

$$G(x,y) = \kappa e^{\left(\frac{-\left(x^2+y^2\right)}{\sigma^2}\right)}$$ (3.5)

where κ is determined by:

$$\sum_x \sum_y G(x,y) = 1$$ (3.6)

and σ is the surround space constant. Surround intensity information is obtained by 2D convolution of (5) with image A', whose elements are the normalized approximation coefficients $a'_{J,k,l}$ given by (3.4) such that:

$$A_f(x,y) = A'(x,y) * G(x,y) = \sum_{x'=-\frac{M}{2}}^{\frac{M}{2}} \sum_{y'=-\frac{N}{2}}^{\frac{N}{2}} A'(x-x', y-y')G(x',y')$$ (3.7)

The ratio between A' and A_f determines whether the magnitude of center coefficient is higher than the average surrounding intensity or not. If it is higher, the corresponding coefficient will be increased, otherwise it will be lowered. As stated above, the size of the surrounding, which has a direct effect on the contrast enhancement result, is controlled by the space constant σ of the surround function G. The local contrast enhancement is carried out as follows:

$$A_{new} = \begin{cases} 255\,\overline{A}\,R\,2^J & \textbf{for } R < 1 \\[2em] 255\,\overline{A}^{\,(\frac{1}{R})}\,2^J & \textbf{for } R > 1 \end{cases} \tag{3.8}$$

where, R is the centre/surround ratio, $\overline{A}$ is the matrix whose elements are the output of the hyperbolic sine function given in (3.3) and A_{new} is the new coefficient matrix which will replace the approximation coefficients $a_{J,k,l}$ obtained by the decomposition of the original image at level J. R is given by:

$$R = \left(\frac{A'}{A_f} \right)^d \tag{3.9}$$

with the parameter d which is an enhancement strength constant with a default value of 1. It can be tuned for an optimal result. When it is greater than 1, the result contrast will be high with a cost of increased noise. When it is less than 1, the resulting image will have less contrast with less noise. The result of the contrast enhancement algorithm after taking the inverse WT of the modified coefficients and applying a linear color restoration process is given in Figure 3.2(c). 1D comparison of the dynamic range compression and the contrast enhancement results are also shown in Figure 3.3. The curves in Figure 3.3 show the average intenstity variations along columns (Figure 3.3(a)) and along rows (Figure 3.3(b)) of the original, dynamic range compressed and contrast enhanced intensity (gray-level) images given in Figure 3.2, respectively. It is observed in Figure 3.3

that the luminance enhancement is achieved by the dynamic range compression and the resulting contrast loss is restored or even improved by the contrast enhancement technique.
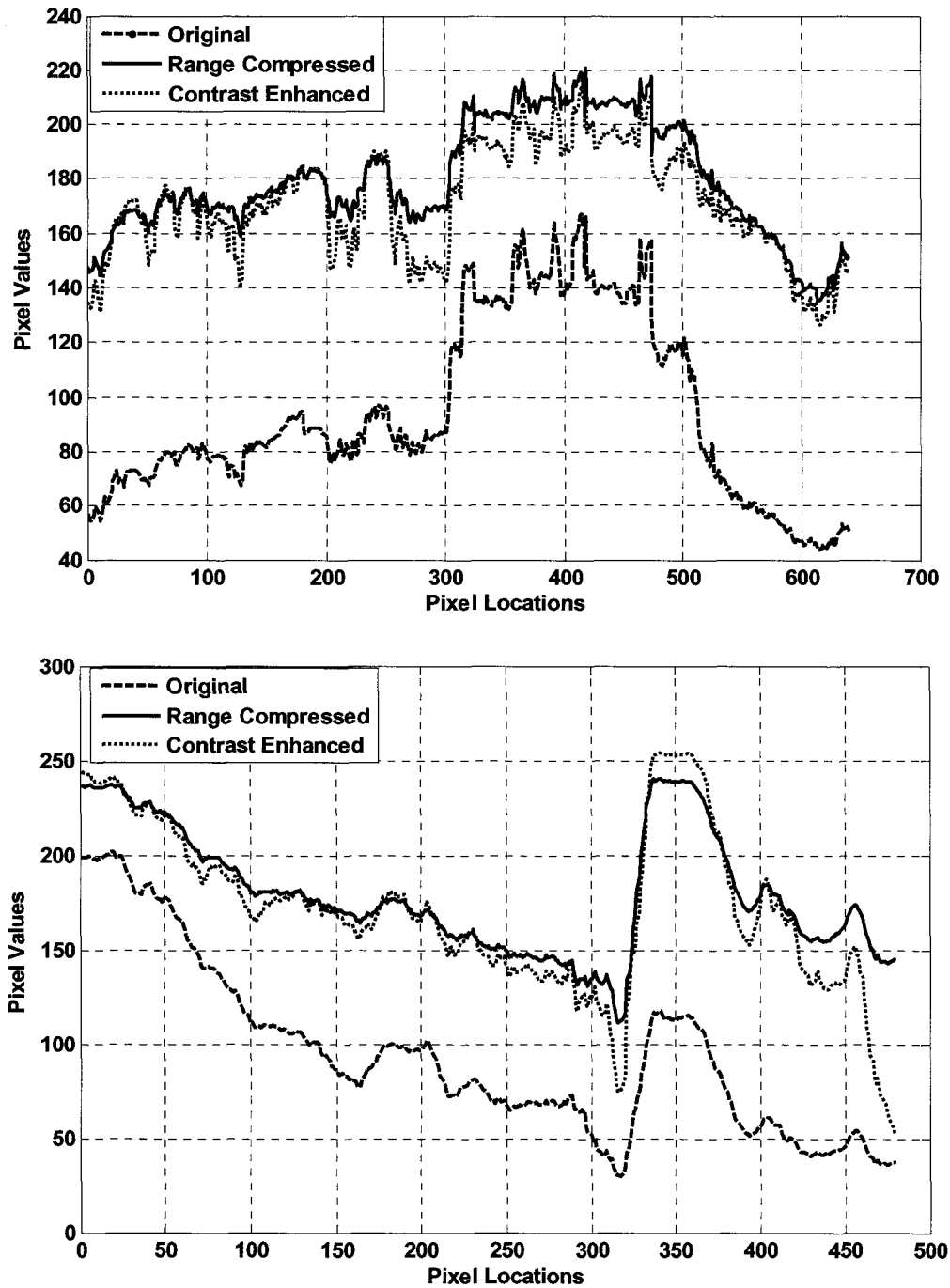

Figure 3.3. Average intensity variations. Top: Across columns;
Bottom: Across rows of the images given in Figure 3.2.

The contrast enhancement transformation given in (3.8) consists of two different equations: the first is an adaptive multiplicative gain and it is used when the centre/surround ratio is less than 1. Multiplication with such a number will decrease the coefficients. The second equation is an adaptive power transform with different values for each coefficient and is valid when the center coefficient is greater than the local average. Since the coefficients are normalized to [0,1] and the term ($\frac{1}{R}<1$) is always satisfied, the power transform given in (3.8) will always produce a higher value but less than or equal to 1. This prevents saturation and halo errors that would occur if the first equation in (3.8) was used instead. The second equation could be used instead of the first one as in AINDANE, but it would not provide as much contrast enhancement as the multiplicative gain.

Using a single scale is incapable of simultaneously providing sufficient dynamic range compression and tonal rendition [29]-[31], therefore different scale constants (e.g. small, medium, large) of the Gaussian kernel can be used to gather surround information and the contrast enhancement process given by (3.5)-(3.9) is repeated for each scale. The final output is a linear combination of the new coefficients calculated using these multiple scales. This needs three times more calculations compared to using only one scale. Instead of using three convolutions, the same result can be approximated using a specifically designed Gaussian kernel [40]. Such a kernel, which we name 'Combined-scale Gaussian (CG)' is a linear combination of three kernels with three different scales:

$$G(x,y) = \sum_{k=1}^{3} W_k K_k \cdot e^{\left(\frac{-\left(x^2+y^2\right)}{\sigma_k^2}\right)}$$

(3.10)

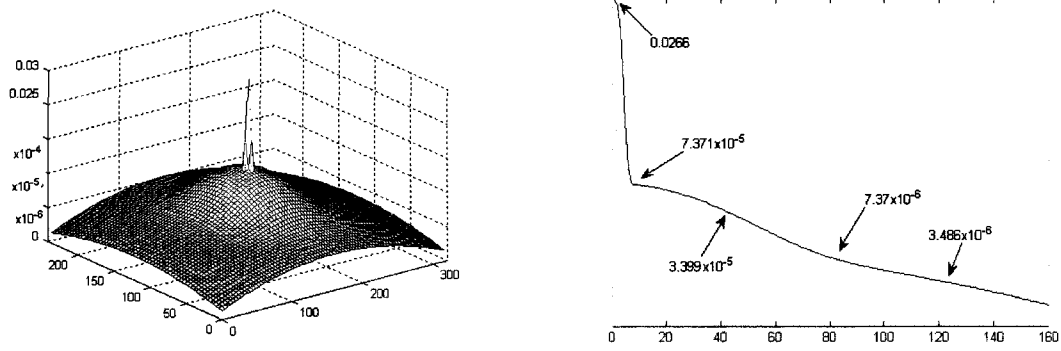with $W_k = \frac{1}{3}$. The CG kernel obtained using three scales (2, 40, 120) is shown in Figure 3.4.

$$D^h{}_{new} = \frac{A_{new}}{A} D^h \qquad D^v{}_{new} = \frac{A_{new}}{A} D^v \qquad D^d{}_{new} = \frac{A_{new}}{A} D^d \qquad (3.11)$$

where A and A_{new} are the original and enhanced approximation coefficients at level 1, respectively. D^h, D^v, D^d are the detail coefficient matrices for horizontal, vertical and diagonal details at level 1, and $D_{new}{}^h, D_{new}{}^v, D_{new}{}^d$ are the corresponding modified matrices, respectively. If the wavelet decomposition is carried out for more than one level, equation (3.12) is used:

$$D^h{}_{new,j} = \frac{A_{new,j}}{A_j} D_j{}^h \qquad D^v{}_{new,j} = \frac{A_{new,j}}{A_j} D_j{}^v \qquad D^d{}_{new,j} = \frac{A_{new,j}}{A_j} D_j{}^d \qquad (3.12)$$

with $j=J,J-1,....2,1$. Here A_j and $A_{new,j}$ is determined by one level reconstruction using A_{j+1} and D_{j+1} for A_j ; $A_{new,j+1}$ and $D_{new,j+1}$ for $A_{new,j}$ at each step. Applying the wavelet algorithm more than once is computationally inefficient. In the implementations one level decomposition for illumination estimation yielded fast results with high visual quality. In Figure 3.2(c)–(d) results obtained with and without detail coefficient modification are given. The need for this step and the impact of the detail coefficient modification is apparent in two examples given in Figure 3.5.

3.5 Color Restoration

A linear color restoration process can be used to obtain the final color image. The ratio between the original and enhanced luminance image, along with the chromatic information of the original image determine the RGB values of the enhanced color image $I_{enh,i}(x,y)$:

$$I_{enh,i}(x,y) = \frac{I_{enh}(x,y)}{I(x,y)} I_i(x,y) \qquad i = r,g,b \qquad (3.13)$$

where $I(x,y)$'s are the pixel values of the input intensity image at (x,y) and is determined by (3.1); $I_i(x,y)$'s are the RGB values of the input color image at the corresponding pixel locations and $I_{enh}(x,y)$'s are the resulting pixels of the enhanced intensity image derived from the inverse wavelet transform of the modified coefficients.
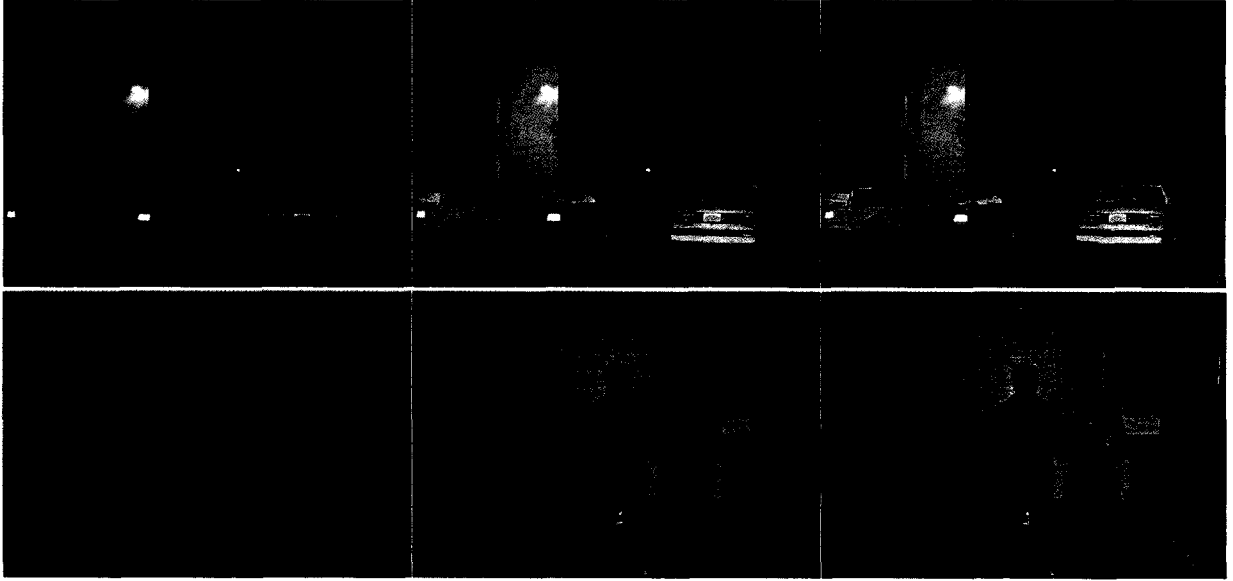
Figure 3.5 Examples showing the effect of detail modification. Original images left, enhancement results without and with detail coefficient modification, middle and right images, respectively.

3.6 Experimental Results

The proposed algorithm has been applied to process numerous color images captured under varying lighting conditions. Digital images used for experiments throughout the dissertation research are either taken with a simple commercial camera or obtained from publicly available internet resources. From observations, it can be concluded that the algorithm is capable of removing shades in high dynamic range images while preserving or even enhancing the local contrast. Besides, the produced colors are consistent with the colors of the original images.
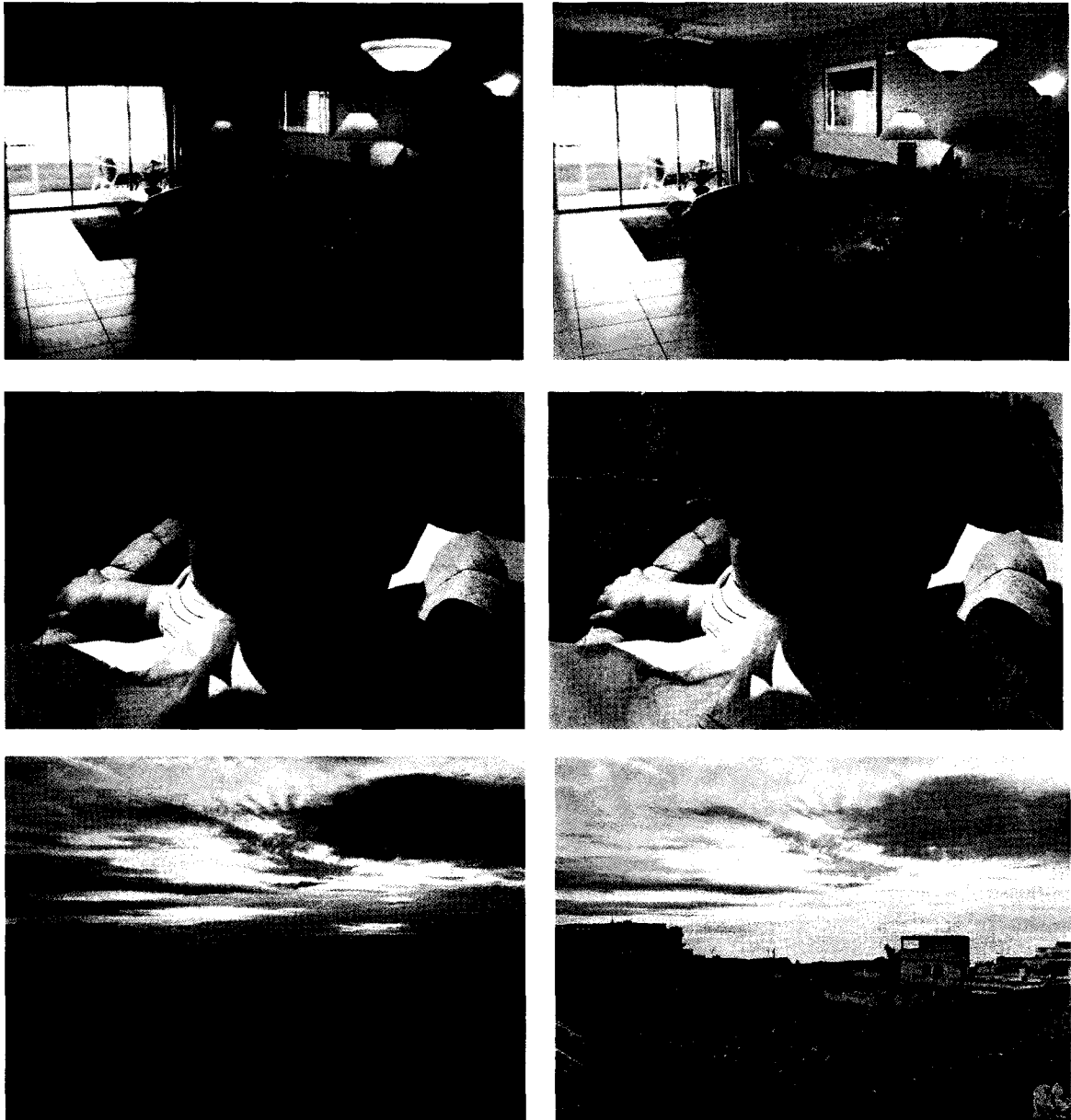
Figure 3.6 Image enhancement results by proposed algorithm. Left column: Original images; Right column: Enhanced images.

Examples given in Figure 3.6 show that the proposed enhancement algorithm is capable of removing shadows and providing better results in terms of visual quality. The local contrast is preserved, even improved, in all these examples. The processed images are sharper than the original ones. Figure 3.7 shows two examples of the real-world scenes that violate the gray-world assumption. Although the scenes are dominated by one color channel (mostly-green), the proposed enhancement algorithm can provide results having very appealing color rendition and not suffering from graying-out of the uniform areas.
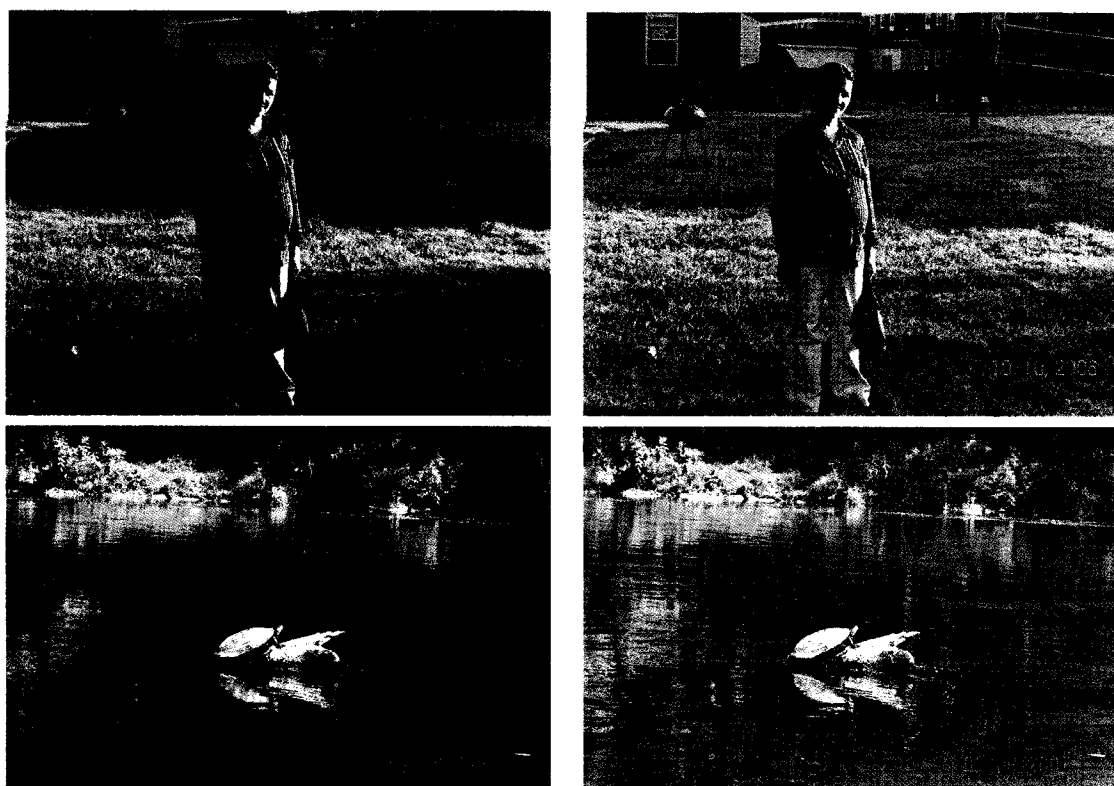
Figure 3.7 Image enhancement results by proposed algorithm. Left column : Original images; Right column: Enhanced images.

Two examples of scenes that have very rich color mixture are given in Figure 3.8. The illumination is also balanced in both scenes. Both enhancement results preserve the color information well, providing sharper results. The background that has low illumination in the first image becomes more visible with realistic and balanced colors in the enhanced image. Both enhanced images are brighter than the original ones.
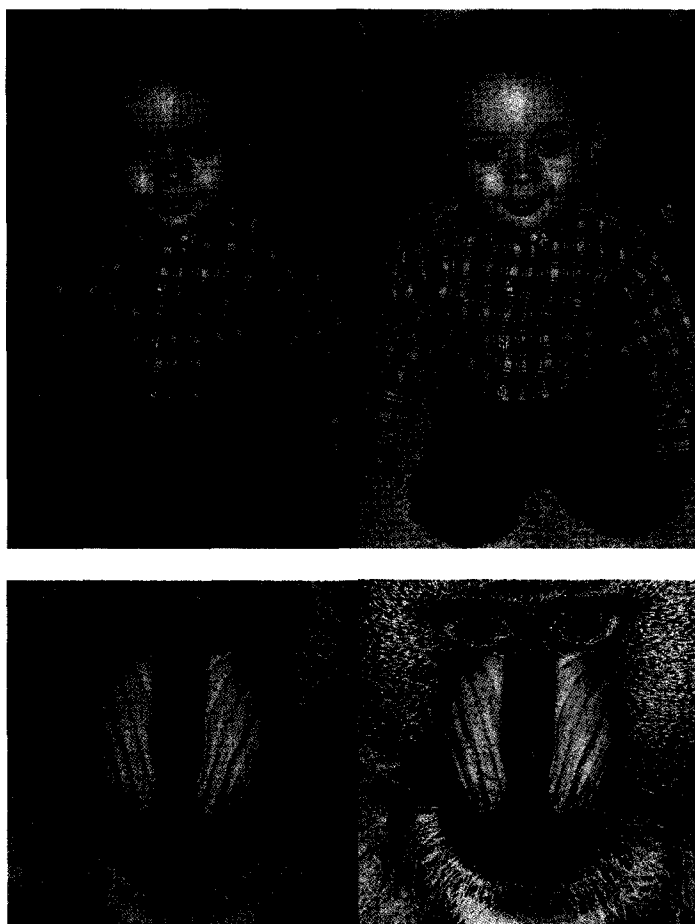
Figure 3.8   Image enhancement results by proposed algorithm. Left column: Original images; Right column: Enhanced images.

The WDRC algorithm successfully accomplishes color rendition, dynamic range compression with local contrast enhancement simultaneously except for some "pathological" scenes that have very strong spectral characteristics in a single band. Two examples for such scenes are given in Figure 3.9. Although the enhanced results are

sharper than the original images and the colors of the enhanced results are consistent with the colors in the original images, they are not the colors observed in real-life scenes. This drawback of the proposed algorithm is shared with AINDANE and IRME as well, since these algorithms, like the proposed one, exploit only the luminance component of the image to be enhanced. The "pathology" in the original image is inherited to the enhanced image via linear color restoration process. The algorithm is not "color constant". Color
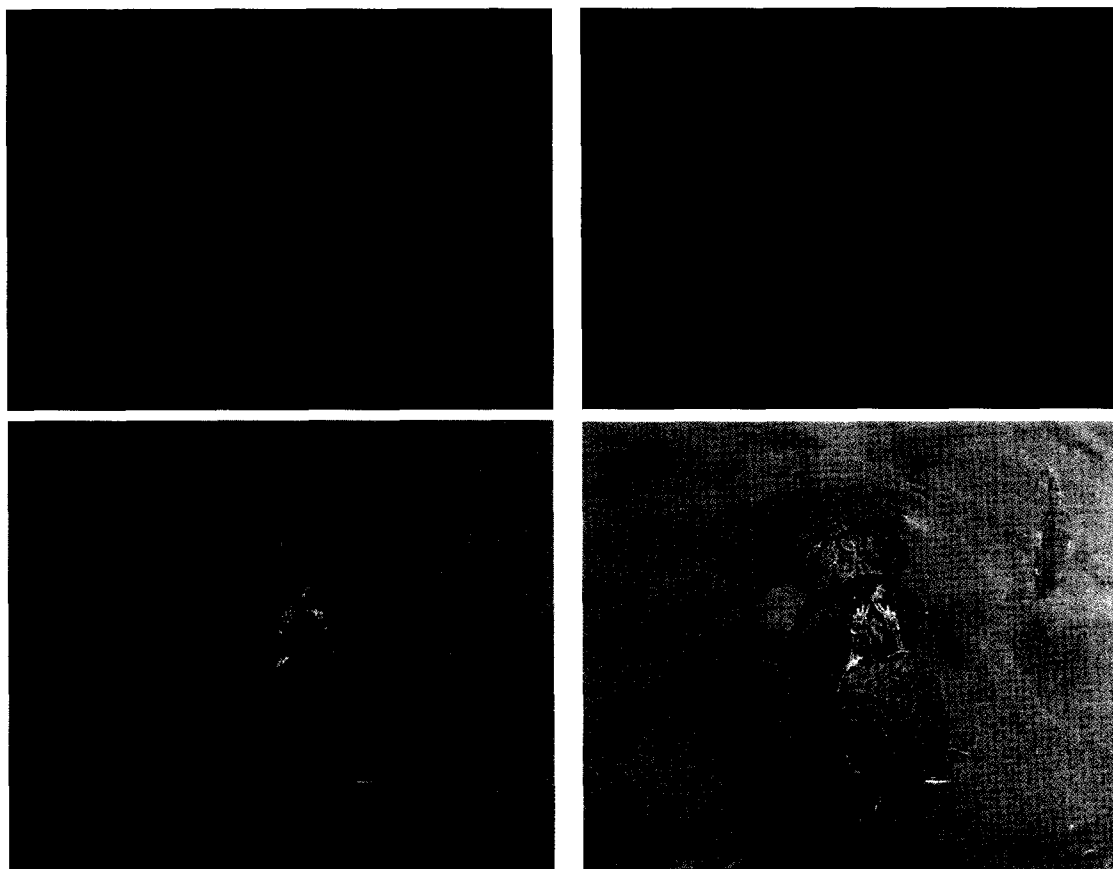
Figure 3.9   Enhancement results of the "Pathological images". Left column: Original images; Right column: Enhanced images.

constancy implies the observed scene is independent of the spectral characteristics of the illumination to some extent. The scenes in given examples would let the real-world colors be more visible. Even though WDRC produces satisfactory results for most natural scenes, it cannot discount the illuminant spectral effect due to previously mentioned

reasons. Hence, a different approach, which will be introduced in the next Chapter is required for the final color restoration process.

3.7 Summary of the Chapter

In this chapter, a new wavelet-based image enhancement algorithm for improving the visibility of low quality digital images is introduced. The proposed enhancement algorithm works on the luminance channel and made up of several steps, some are applied in discrete wavelet domain. In the implementation of the algorithm, first a luminance enhancement via dynamic range compression of approximation coefficients obtained from the wavelet transform of the original image data is proposed. Second, a local contrast enhancement process using averaged luminance information of neighboring pixels which is inherited to approximation coefficients is applied. Then, detail coefficients are modified according to the degree of the enhancement of the approximation coefficients, and finally a linear color restoration process to recover the original color of the image. The algorithm provides dynamic range compression, local contrast enhancement, and color rendition simultaneously for a large variety of natural images except for some "pathological" scenes that have very strong spectral characteristics in a single band and for extremely turbid images.

CHAPTER IV

WAVELET-BASED DYNAMIC RANGE COMPRESSION AND LOCAL CONTRAST ENHANCEMENT WITH COLOR RESTORATION

4.1 Introduction

As stated in the previous Chapter, the colors of the enhanced images produced by the WDRC algorithm are consistent with the colors of the original image, but fails to produce color constant results for some "pathological" scenes that have very strong spectral characteristics in a single band. The color restoration process which maps the ill conditioned recorded scene illuminant spectral distribution in the original image linearly to the enhanced image, is the main reason for this drawback. For tackling the color constancy problem, a novel technique was developped. The illuminant is modeled with an effect on the image histogram as a linear shift and the image histogram is adjusted to discount the illuminant. The WDRC algorithm is then applied with a slight modification, i.e. instead of using a linear color restoration, a color restoration process employing the spectral context relationships of the original image similar to the process introduced in Jobson *et al.* [31] and Rahman *et al.* [33] is applied. The scheme of the algorithm is shown in Figure 4.1.

| Image Histogram Adjustment in each Spectral Channel | → | WDRC Enhancement Algorithm | → | Non-linear Color Restoration |
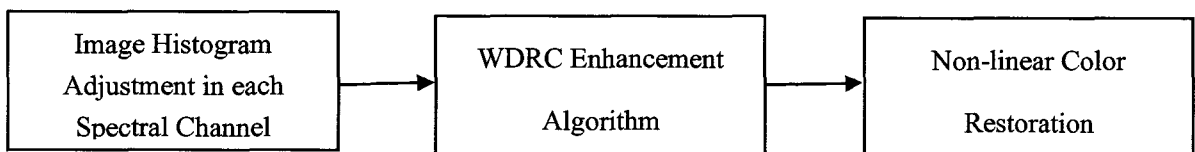
Figure 4.1 WDRC+Color Restoration

4.2 Proposed Color Restoration

The proposed color restoration process consists of the separate steps as depicted in Figure 4.1.

1. Histogram adjustment in each spectral channel of the input image before processing with WDRC algorithm.

2. Producing the triplets values of the enhanced image via a non-linear color restoration.

4.2.1 Histogram Adjustment

The motivation in making a histogram adjustment for minimizing the illumination effect is based on some assumptions about image formation and human vision behavior. The sensor signal $S(x,y)$ incident upon an imaging system can be approximated as the product [22]:

$$S(x,y) = L(x,y)R(x,y), \tag{4.1}$$

where $R(x,y)$ is the reflectance and $L(x,y)$ is the illuminance at each point (x,y). In lightness algorithms, assuming that the sensors and filters used in artificial visual systems possess the same nonlinear property as human photoreceptors [22], i.e., logarithmic responses to physical intensities incident on their photoreceptors (4.1) can be decomposed into a sum of two components by using the transformation $I(x,y) = \log(S(x,y))$:

$$I(x,y) = \log(L(x,y)) + \log(R(x,y)), \tag{4.2}$$

where $I(x,y)$ is the intensity of the image at pixel location (x,y). (4.2) implies that illuminance has an effect on the image histogram as a log-linear shift. This shift, intrinsically, is not the same in different spectral bands.

Another assumption of the lightness algorithms is the gray-world assumption stating that "*the average surface reflectance of each scene in each wavelength band is the same:*

gray" [22]. From an image processing stance, this assumption indicates that images of natural scenes should contain pixels having almost equal average gray levels in each spectral band.

Combining (4.2) with the gray-world assumption, a histogram adjustment is performed as follows:

1. The amount of shift corresponding to illuminance is determined from the beginning of the lower tail of the histogram such that a predefined amount (typically 0.5%) of image pixels is clipped.

2. The shift is subtracted from each pixel value.

3. This process is repeated separately for each color channel.

4.2.2 Non-linear Color Restoration

Jobson *et al.* [29,31] consider a colorimetric transform as a starting point, using ratios that are less dependent on illuminant than raw spectro-photometry. They use the following color restoration factor (CRF) to achieve the desired rendition:

$$\alpha_i = \lambda \log \left(I_i(x,y) \Big/ \sum_{i=1}^{N} I_i(x,y) \right) + \zeta$$

(4.3)

where λ and ζ are canonical color gain and color offset values respectively, and α_i is multiplied with the output of the MSR to produce the color restored MSRCR output. The α_i factor solves the problem of the graying of areas of constant intensities in MSR processed images [29-31]. Application of this factor, along with its impressive results lead to the conclusion that the visual information is not only the log of spatial context relationships within the image but the spectral context relationships as well.

Inspired by MSRCR, a non-linear approach was used to obtain the WDRC output. The CRF given in (4.4) is different from the one used in the MSRCR technique in such a way that in computing the spectral context ratios only the maximum spectral channel intensity at the pixel location *(x,y)* is used instead of adding each channel intensity. Instead of using a logarithmic function a canonical gain is applied as a power transform to the ratios. It should also be emphasized that one more distinction of the CRF from the CRF of MSRCR is that in MSRCR (4.3) is applied to each color channel of the MSR processed images while in WDRC-CR (4.4) is applied to the output intensity image enhanced by WDRC without any color restoration process.

The CRF is determined empirically as in MSRCR after trying several color restoration functions on a range of test images. It is given by:

$$I_{enh,i} = \alpha_i I_{enh}, \alpha_i = \left(I_i(x,y)/\max(I_i(x,y))\right)^{\beta}.$$

(4.4)

where β is the non-linear gain factor corresponding to the canonical gain of CRF in MSRCR. When β is equal to one the color restoration factor will be same as the linear color restoration of the WDRC. This factor has a canonical value as in MSRCR and increases the color saturation resulting in a more appealing color rendition.

4.3 Experimental Results

The WDRC+CR algorithm has been applied to process many different color images of various types, some of which are taken with a standard consumer camera or gathered from the internet site [38]. From observations, it can be concluded that the algorithm is capable of removing shadows in the high dynamic range images while preserving or even enhancing the local contrast well. Additionally, it produces almost color constant results much as HVS does. In this chapter, some results obtained by the proposed algorithm that demonstrate its ability to produce dynamic range compressed images while preserving local contrast, color constancy, and appealing rendition are shown.

In Figure 4.2, a computer simulated red, green, and blue illumination is applied to the mandrill image. The second row shows the histogram-adjusted images, and the third row shows the WDRC processed images of the second row. Histogram adjustment discounts the illuminant to a significant degree, mimicking the HVS, whose color constancy mechanism does not completely discount illumination variations. Overall enhancement results are brighter and sharper than the images of both rows.

Fidelity, F, is a measure of similarity between two images and given by

$$F(I_1, I_2) = 1 - \frac{\sum\limits_{x=0}^{M-1}\sum\limits_{y=0}^{N-1}(I_1(x,y) - I_2(x,y))^2}{\sum\limits_{x=0}^{M-1}\sum\limits_{y=0}^{N-1}(I_1(x,y))^2} \qquad (4.5)$$

Fidelity between an image and itself is 1. In Table 4.1 fidelity results between the original image and the images shown in Figure 4.2 is given. Notice that histogram adjustment increases fidelity 2-3%, showing the impact of the process on discounting the illumination variations. The results given in the third row show the fidelity between the WDRC processed results of the original image and the images shown in the second row of Figure 4.2. WDRC processed images have fidelity near to 1, indicating the ability of the proposed algorithm in producing color constant results.

Table 4.1 Fidelity experiments. First row: Fidelity between original and simulated images. Second row: Fidelity after histogram adjustment. Rows 3-6: Fidelity between the processed original and the processed simulated images. The image enhancement algorithms given in the last column are used to enhance the original and simulated images.

	Red Illuminated	Green Illuminated	Blue Illuminated	Algorithm
F	0.9517	0.9666	0.9435	-
	0.9721	0.9839	0.9797	Histogram Adjusted
	0.9933	**0.9941**	**0.9927**	**WDRC+CR**
	0.9639	0.9673	0.9606	MSRCR
	0.9604	0.9691	0.9493	IRME
	0.9679	0.9768	0.9610	AINDANE
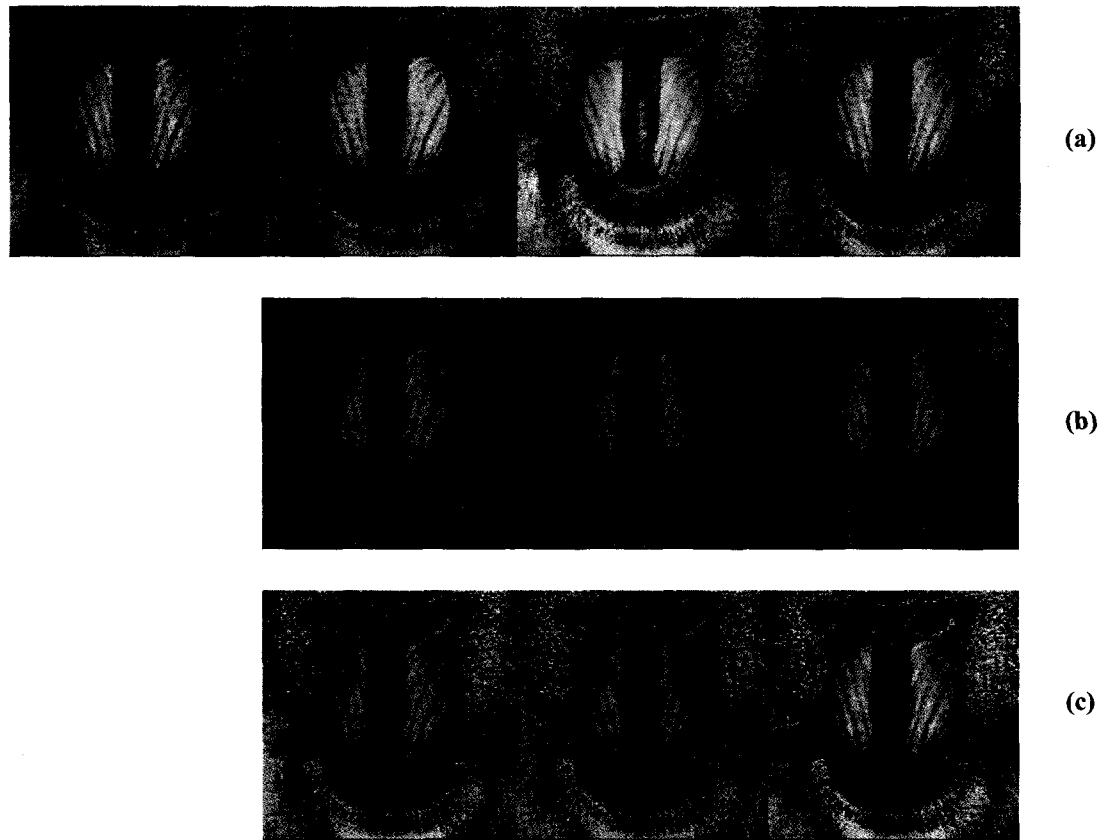
Figure 4.2 The impact of WDRC+CR on discounting the illumination. (a) Simulated mandrill images with red, green, and blue illumination, respectively. (b) Histogram adjusted images obtained from the images of first row. (c) WDRC-CR applied to images of the second row. Illumination simulations are obtained using PhotoFlair®, a commercial image processing software. Top left: Original image.

Figure 4.2, along with Table 1, show comparisons between WDRC+CR and other non-linear image enhancement algorithms: MSRCR, IRME, and AINDANE. The original image and illumination-simulated images are enhanced with various algorithms. MSRCR images are produced using PhotoFlair®, commercial software, with the default settings except for "white-balance" turned off and IRME and AINDANE results are produced with default settings using MATLAB codes provided by the authors. Fidelity results between the processed original and processed simulated images show superiority of the proposed algorithm in producing color constant results. The enhanced results depicted in Figure 4.3 show this similarity between the WDRC + CR enhanced images for all type of simulations.
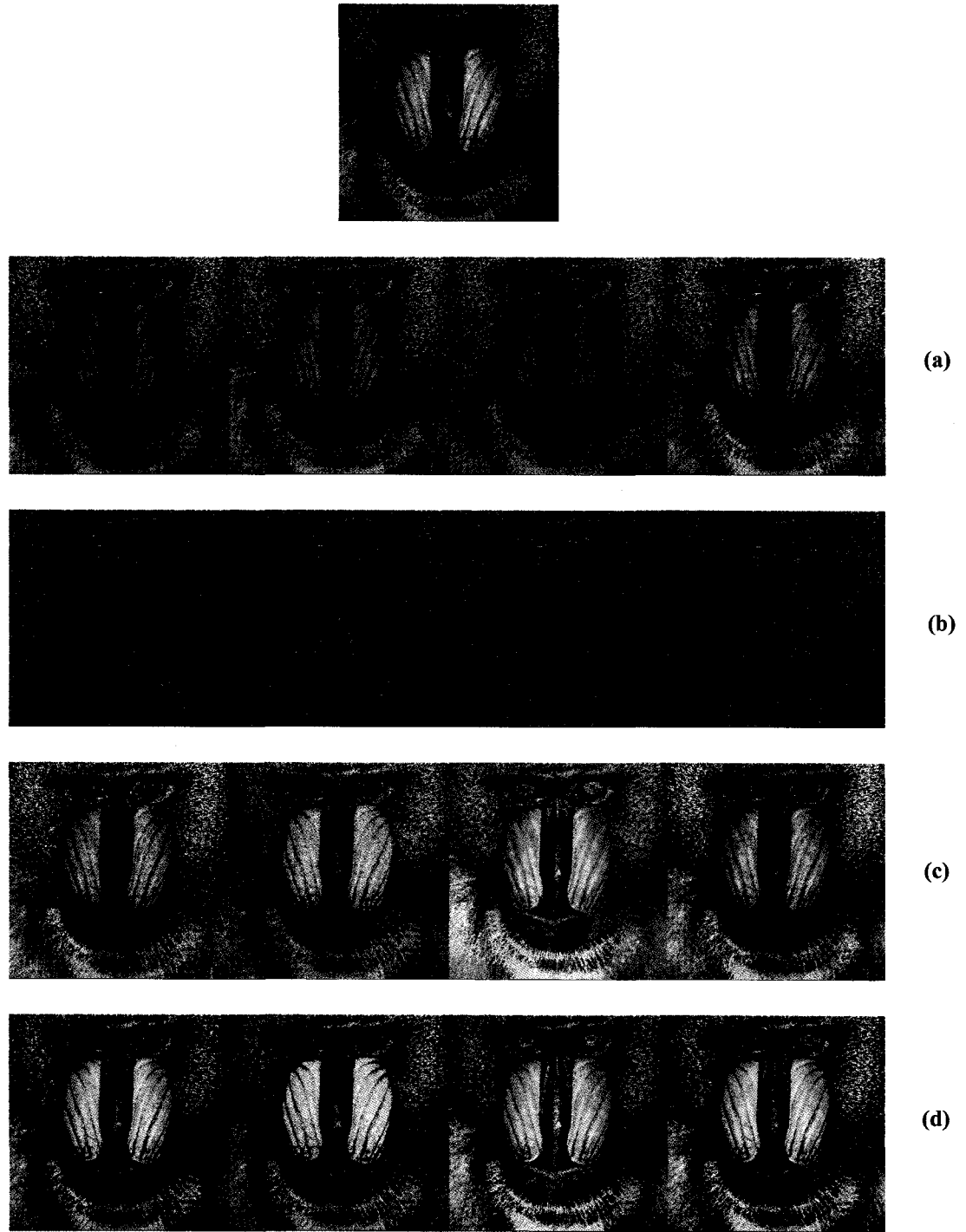
Figure 4.3. Enhancement results of algorithms applied to original and simulated images given in Figure 4.2.
(a) WDRC+CR (b) MSRCR (c) IRME (d) AINDANE results. The topmost image is the original.

Among the enhancement algorithms, MSRCR and AINDANE show an evident contrast enhancement. The contrast enhancement of AINDANE is severe causing blackening of an

important amount of pixels, while IRME has the poorest local contrast with increased average luminance resulting in a hazy appearance. WDRC+CR seems to produce the most balanced results in terms of increased local average intensity and increased local contrast.

The proposed algorithm produces successful results even for the "pathological" scenes that have very strong spectral characteristics in a single band. Two examples for such scenes are given in Figure 4.4. Notice that WDRC+CR is capable of removing the illumination defect in both scenes recovering the original colors, while WDRC can't perform well enough to discount the illuminant defect.

Three more examples for scenes that have very rich color mixture are given in Figure 4.5. The illumination in each scene differs from each other such that the scene in Figure 4.5(a) has a diffused illumination causing a hazy appearance and saturation, the scene in Figure 4.5(b) has a non-uniform illumination because of the shadow cast by the truck, and the scene in Figure 4.5(c) has a dark and defocused background due to insufficient illumination and distance, respectively. The final results preserve the color information well, providing a sharper appearance. The haze is removed in the first example, the shadow is eliminated in the second example, and the blurred and dark background becomes sharper and more visible with realistic and balanced colors in the third example. All of the enhanced images are brighter than the original ones.

The WDRC+CR algorithm successfully accomplishes color rendition and dynamic range compression with local contrast enhancement simultaneously even for "pathological" scenes that have very strong spectral characteristics in a single band. It overcomes the drawback of WDRC, which is also encountered in other enhancement algorithms like AINDANE and IRME in which algorithms perform only the luminance component of the image and the final color image is determined via a linear color restoration process. The proposed algorithm produces "color constant" results, discounting the impact of the illumination variations. The observed scenes in given examples have similar colors to those produced by WDRC+CR.

(a)

(b)

(c)

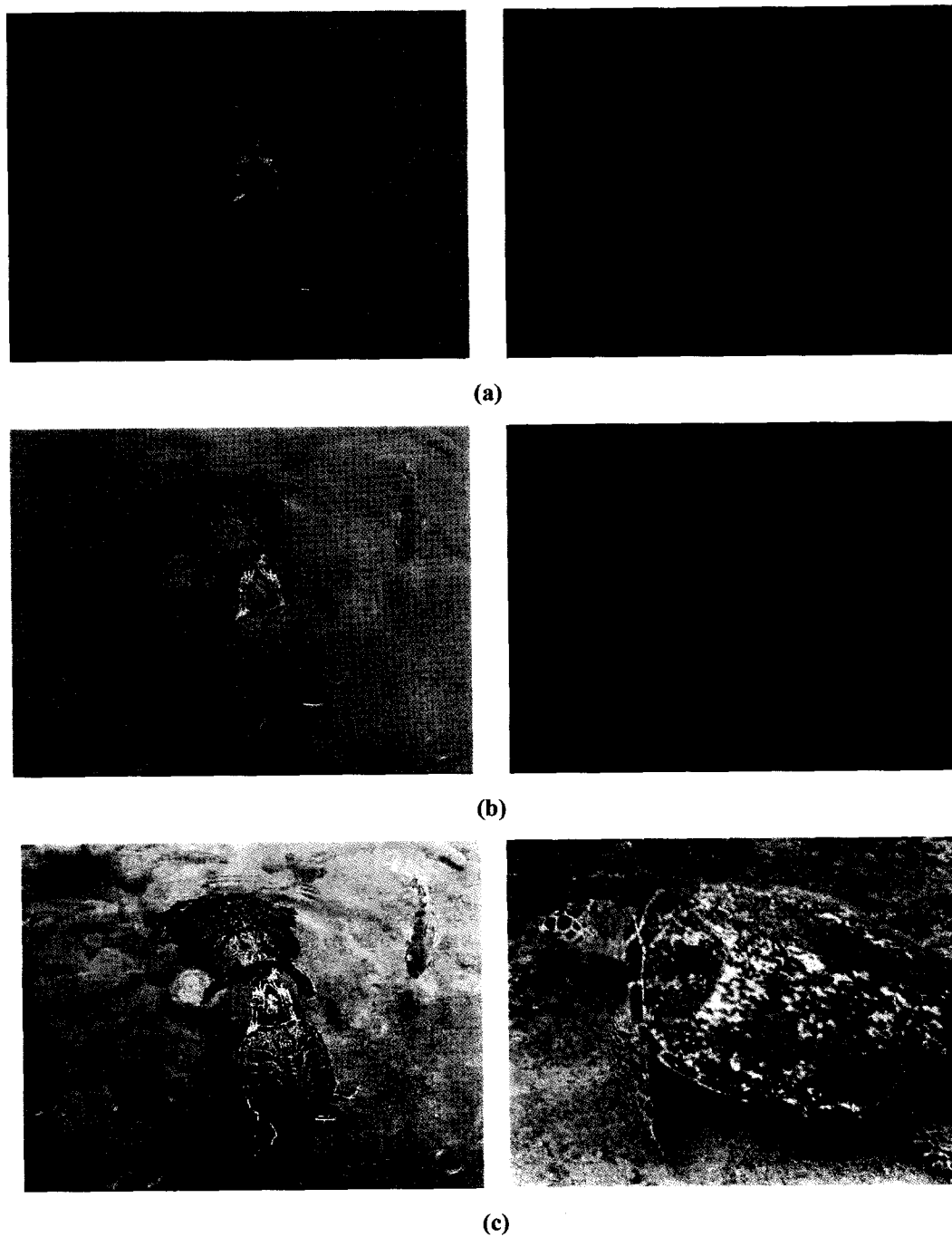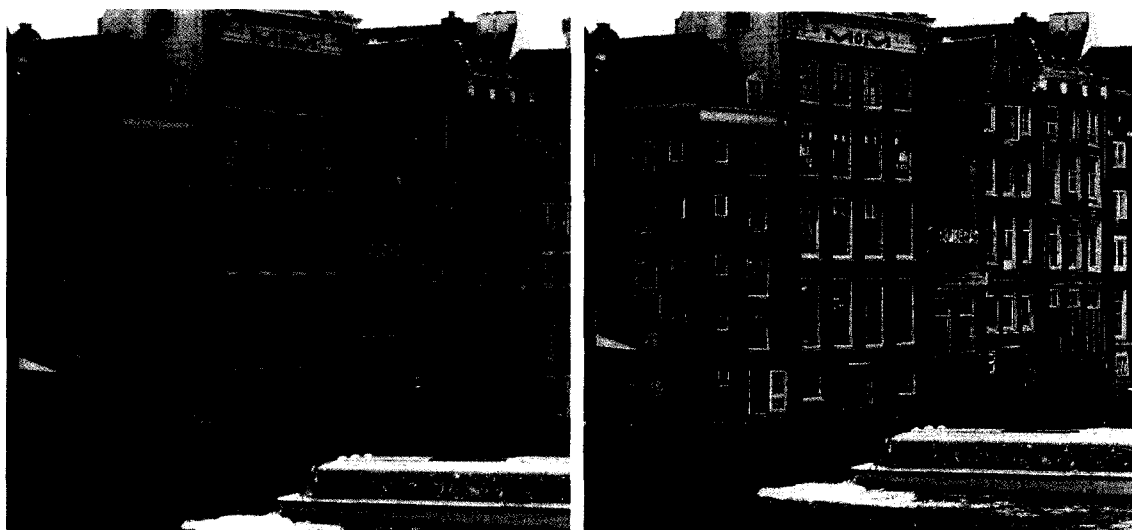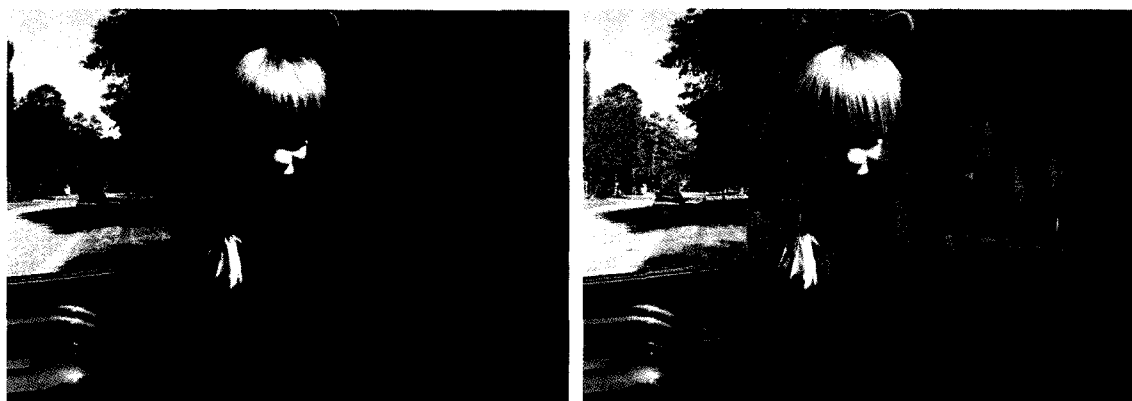**Figure 4.4** Enhancement results of the "pathological images." (a) Original images; (b) WDRC enhanced images; and (c) WDRC+CR enhanced images

Figure 4.5 Results obtained with WDRC+CR. Left column: Original images; Right Column: Enhanced images.

The WDRC-CR algorithm has also been applied to numerous aerial images with different degree of turbidity to show its potential usage in aerial imagery. The results show improved clarity i.e. the increased visibility distance for haze, fog, clouds and heavy rain. The algorithm works well for images captured in diverse flight conditions. Some examples for such conditions are presented in Figure 4.6. The left column in the figure depicts the original images and right column shows the enhanced WDRC-CR results. The example in Figure 4.6(a) shows a scene with mild haze; the proposed algorithm completely removes the haze resulting in sharper image with saturated colors. The scene in Figure 4.6(b) suffers from moderate fog with some smoke. Good clarity is achieved and the colors of the scene content are restored in the enhanced image. In Figure 4.6(c) an example of scenes with clouds and thick fog causing thicker turbidity is depicted. In the enhanced image visibility of features is improved significantly. Figure 4.6(d) is an example of a scene with near zero visibility. The enhanced images achieve a high level of improvement to feature visibility removing the severe turbidity

In Figure 4.7 a comparison of the proposed algorithm with MSRCR, AINDANE[42], IRME [43], and LTSN [45] is given. MSRCR enhanced images are obtained using the default settings of PhotoFlair® with white balance preference turned-off. AINDANE, IRME, and LTSN results are produced using MATLAB codes with default settings, provided by the authors. Results from so-called autolevels enhancement* of the original image as well as the MSRCR processed images are also given to show the superiority of the proposed algorithm. From Figure 4.7 and from the experiments conducted with many other images, it can be inferred that the proposed algorithm outperforms these algorithms, providing better visibility enhancement and rendition simultaneously.

---

*Autolevels is a global image enhancement technique in which image histogram is stretched linearly after some portion of its both tails are clipped. For images with narrow histograms autolevels performs quite well and produces globally contrast enhanced images.
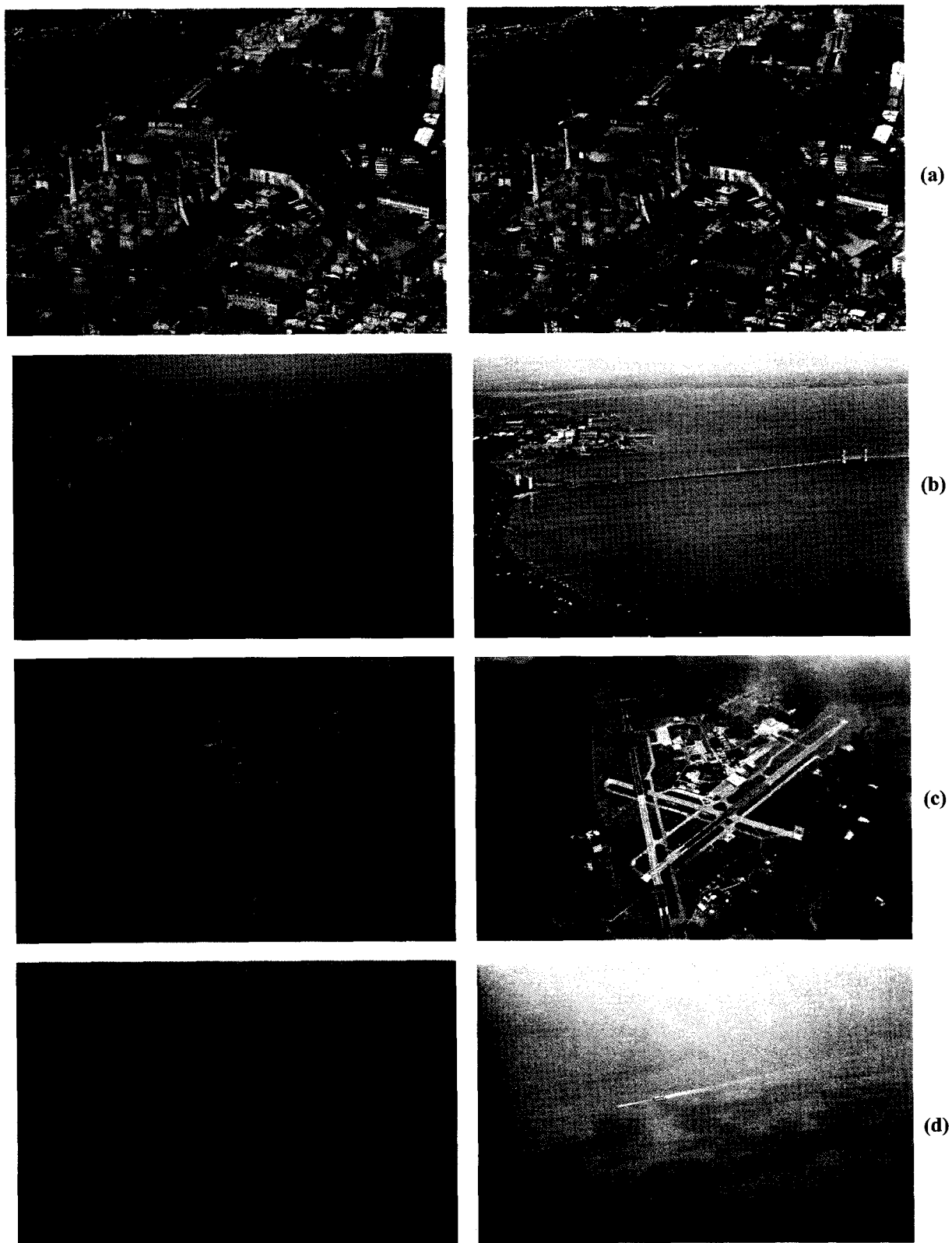
Figure 4.6 The enhancement results for different types of turbidity.
Left column: Original images; Right column: Enhanced images.
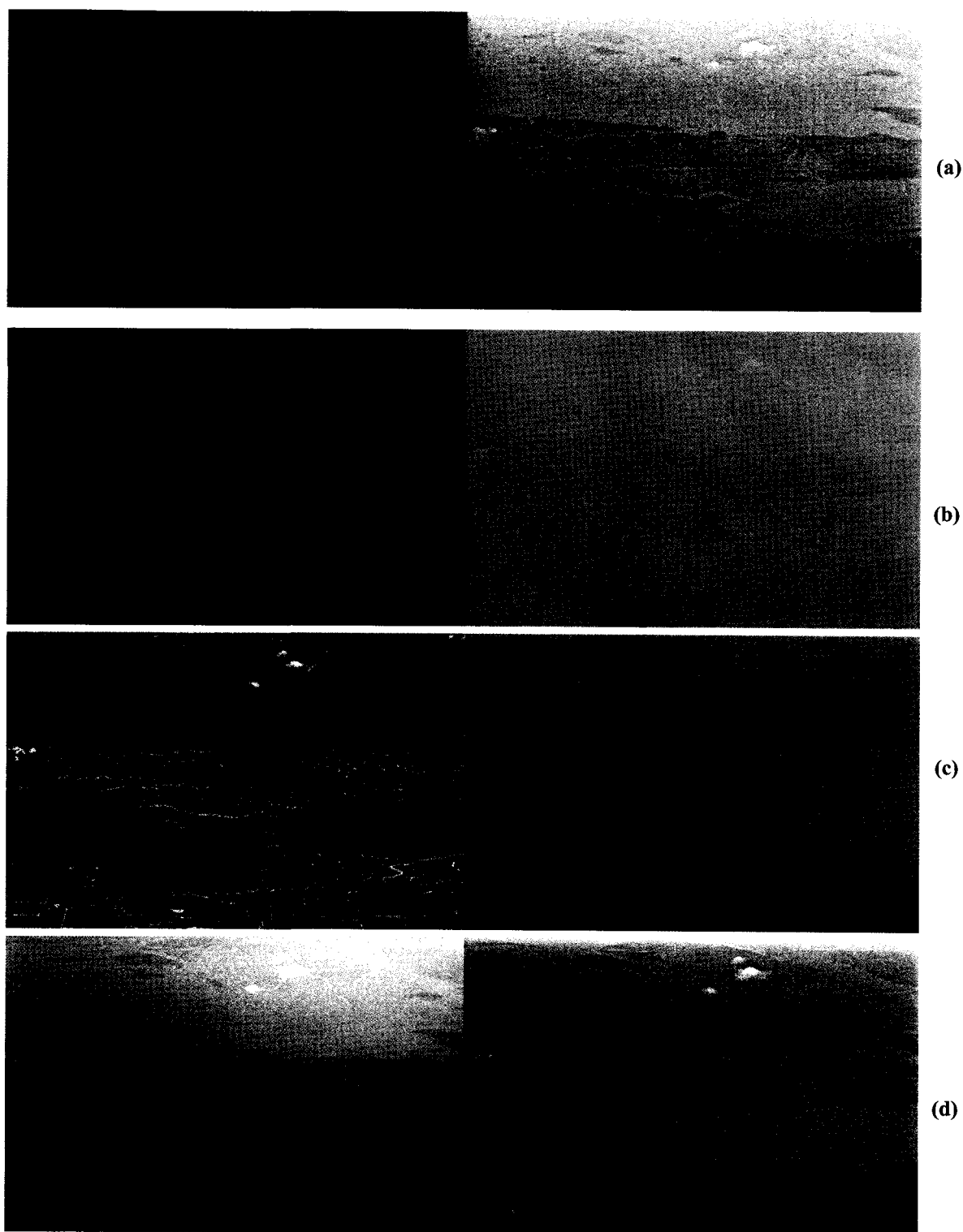
Figure 4.7 Comparison of the proposed algorithm with other techniques. Left column, **(a)** to **(d)**: Original, AINDANE, LTSN, Autolevels. Right column, **(a)** to **(d)**: Proposed method, IRME, MSRCR, MSRCR+Autolevels, respectively.

4.4 Computational Complexity

In previous sections, some comparisons of the WDRC-CR processed images with the results of other retinex inspired enhancement techniques were shown. In this section, the computational complexity of the proposed algorithm is briefly discussed and is compared with its retinex based relatives: MSRCR, AINDANE, and IRME. Since the algorithms used for comparisons are written on different environment with less or more code optimization; run time comparisons would not lead to fair results. Instead of giving run times for each algorithm, the computational complexities of the algorithms are calculated.

The retinex based algorithms which use the centre/surround ratio in some fashion in their computations, calculate the surround using discrete spatial convolutions of the input images with Gaussian kernels of different scales. Because of high dimensionality of the convolutions, those are realized in Fourier domain by transforming the input image and the kernels with fast FT (FFT)'s, multiplying FFT transformed data and taking the inverse FFT to get the convolution results. Computations of FFT transforms are the main factors of the computational complexity. In MSRCR, AINDANE and IRME algorithms, full sized images are used in convolutions, while in the proposed algorithm only the approximation coefficients dimensionality of which is reduced by factor 4 (by 2 along rows and by 2 along columns) after one level Fast WT (FWT) of the intensity image are utilized as an input image to convolution. In addition to this, it is important to point out that the MSRCR algorithm, in its default settings, is applied to each color channel separately with three different scales, whereas AINDANE runs only on the intensity image with three scales just as MSRCR, and IRME almost with the same calculations of AINDANE, performs its computations for only one scale of Gaussian surround function. WDRC is also applied on the luminance channel for one scale but with the reduced dimensions.

Recalling the computational complexity of FFT for images with N pixels is $O(Nlog_2N)$ and the complexity of FWT is $O(N)$ with same orders for inverse transforms, the whole computational complexity for each algorithm to produce one pixel of the enhanced image of N pixels in calculated. In these calculations, it is assumed that the Gaussian kernels are produced directly in Fourier domain, so that it is not required to take the forward FT for the Gaussian kernels. For example, in MSRCR algorithm, the number of multiplications contributed to the computational complexity of the algorithm from the convolutions which are realized as FFT domain multiplications for three distinct scales of the surround function will be 9NlogN+9N (3NlogN for the forward FT of the input image for three color channels, 3NlogN for the inverse FT after multiplying each Gaussian kernel produced in Fourier domain with FFT processed color channels of the input image and finally 3NlogN for the inverse FT for three distinct scales). Producing a Gaussian kernel directly in the FT domain requires 8N multiplications and 2N exponentials for each scale and totally 24N multiplications and 6N exponentials for three scales. The overall computational complexity is determined by taking into account the gain/offset and color restoration computations. The computational complexities for the proposed and the other benchmark algorithms are determined in the same way.

The results are given in Table 4.2 showing the pace of the proposed algorithm compared to other retinex inspired algorithms. To see the impact of different non-linear tone-mapping functions on the run time, their run times are measured for ten different 1024 by 1024 sequences and the results are averaged, which is given in Table 4.3. Using the normalized run times of different mapping functions from Table 4.3, computational complexity comparison of the algorithms for different sized input images are given in Table 4.4. From the table, it is seen that proposed WDRC algorithm with linear color restoration is ~10x faster than MSRCR and AINDANE, ~5x faster than IRME, whereas WDRC with histogram adjustment and non-linear color restoration is ~3x faster than

59

MSRCR and AINDANE, ~1.5x faster than IRME which is known to be designed for real time video processing on PC platforms.

Table 4.2 Computational complexities of various retinex inspired algorithms for producing one pixel of the enhanced image of N pixels.

Algorithm	Computational Complexity / Pixel
MSRCR	$O(36+9\log_2 N)$ +4 log function+6 exponential
AINDANE	$O(48+4\log_2 N)$ +6 power transform+6 exponential
IRME	$O(31+2.\log_2 N)+2$ power transform+1 log function+2 exponential
WDRC	$O(13+0.5 \log_2 \frac{N}{4})+0.25$ sinh function+0.125power transform +0.5 exponential.
WDRC-CR	$O(21 + 0.5\log_2 \frac{N}{4})+0.25$ sinh function+3.125 power transform + 0.5 exponential.

Table 4.3 Average run times for ten 1024x1024 length sequences for different mapping functions.

Function	Time	~ Normalized Time
Logarithm	0.2824 sec.	24
Floating point power transform	0.3848 sec.	32
Hyperbolic sine	0.2352 sec.	20
Exponential	0.1659 sec	14
Floating point multiplication	0.0119 sec.	1

Table 4.4 Computational complexities of various retinex inspired algorithms for producing one pixel of the enhanced image of different sizes.

Algorithm/Image Size	256x256	512x512	1024x1024	2048x2048
MSRCR	O(360)	O(378)	O(396)	O(414)
AINDANE	O(388)	O(396)	O(404)	O(412)
IRME	O(179)	O(181)	O(185)	O(189)
WDRC	**O(36)**	**O(37)**	**O(38)**	**O(39)**
WDRC-CR	**O(128)**	**O(129)**	**O(130)**	**O(131)**

4.5 Summary of the Chapter

In this Chapter, a new color restoration approach for solving the color constancy issue of the WDRC method is introduced. The color restoration process which maps the ill-conditioned recorded scene illuminant spectral distribution in the original image linearly to the enhanced image, is the main reason for this drawback. For tackling the color constancy problem a novel technique is proposed. The illuminant is modeled as it has an effect on the image histogram as a linear shift and for discounting the effect of the illuminant, a histogram adjustment process is proposed. Following the histogram adjustment process, the WDRC algorithm is applied for dynamic range compression and local contrast enhancement in the luminance channel except for the color restoration. Finally instead of using a linear process of the WDRC, a non-linear color restoration process employing the spectral context relationships of the original image is applied to the enhanced intensity image to produce the enhanced color images. Experiments conducted with numerous images show that the proposed algorithm provide an appealing rendition and color constancy better than the state-of-the-art methods. The proposed algorithm is also computationally more effective than its relatives.

CHAPTER V

WAVELET-BASED IMAGE INTERPOLATION

5.1 Introduction

In this Chapter, a new wavelet-based image interpolation algorithm is introduced for magnifying the image details so that the visibility is improved. To achieve this aim, the algorithm is performed in the WT domain. In all the related work in literature addressed previously in Chapter 2, the image in hand is considered a low resolution (LR) image, and is treated as the approximation part (i.e. low-pass filtered subband) of an unknown wavelet transformed high resolution (HR) image. If one can estimate the detail coefficients (i.e. the missing high frequency content) accurately, then it will be possible to obtain the unknown HR image by taking the inverse wavelet transform. The proposed interpolation technique also exploits this approach and suggests a simple but efficient estimation for the high pass filtered subbands.

Unfortunately producing the exact HR image is not, in general, possible, especially if aliasing occurs in sampling the captured the scene content. This is a case encountered when the sampling rate is not at least twice the maximum spatial frequency of the scene content. As a result, the high frequency information is mixed up with the data at low frequencies and it will not be possible to get the original data. Nevertheless, the research on developing interpolation methods for estimating HR images that visually and statistically approach the actual HR scene still merits interest.

The proposed interpolation algorithm consists of three distinct steps.

1. An initial HR image of size twice the LR image is estimated using zero padding of the details.

2. The HR image is transformed via UWT resulting in four subbands, namely LL, LH, HL, HH using a non-orthogonal filter bank. The size of each subband is twice the size of the LR image.

3. In the transformed domain LL subband is replaced with the initially estimated HR image and applying the inverse UWT, the final HR image is determined.

In Section 5.2, the mathematical backgrounds of the UWT are presented. In Section 5.3, the implementation of the proposed interpolation is introduced. In Section 5.4, the results from the experiments on the assessment of the method are illustrated including the comparisons with the recent spatial and wavelet domain interpolation techniques along with the classical ones.

5.2 Undecimated Wavelet Transform Using the "à Trous" Algorithm

The most popular WT algorithm, which is also used in JPEG2000, is the standard decimated bi-orthogonal wavelet transform (DWT), since the bi-orthogonal WT gives good results in image compression. However, standard DWT is not optimal for other applications such as filtering, deconvolution, detection, or more generally, analysis of data [91]. The main reason for this is the lack of shift-invariance property in the DWT, which leads to many artifacts when an image is reconstructed after modification of its wavelet coefficients. Therefore an undecimated wavelet transform (UWT) in which the decimation step of the standard DWT is eliminated [92],[93] can be used alternatively for other applications such as denoising. In [95], Starck *et al.* show an improvement by more than 2.5dB in denoising via tresholding application using an undecimated transform instead of the regular one.

The undecimated UWT of a 1D signal c_0, W using the filter bank (h, g) is a set $W=\{w_1, \ldots ,w_J , c_J \}$ where w_j are the wavelet coefficients at scale j and c_J are the coefficients at the coarsest resolution. The "à trous" (meaning 'with holes' in French)

algorithm [92]-[94] can be applied in order to obtain wavelet coefficients at one resolution from another using the following equations:

$$c_{j+1}[l] = \left(\overline{h}^{(j)} * c_j\right)[l] = \sum_k h[k] c_j\left[l + 2^j k\right]$$

$$w_{j+1}[l] = \left(\overline{g}^{(j)} * c_j\right)[l] = \sum_k g[k] c_j\left[l + 2^j k\right] \tag{5.1}$$

where '*' is the convolution operator and $\overline{h}[n] = h[-n], n \in Z$ is the time-reversed of the discrete-time filter with an impulse response $h[n]$ and $h^{(j)}[l] = h[l]$ if $l / 2^j$ is an integer and 0 otherwise. For example when $j=1$,

$$h^{(1)} = (\ldots, h[-2], 0, h[-1], 0, h[0], 0, h[1], 0, h[2], \ldots)$$

The reconstruction of the signal c_j is realized via

$$c_j[l] = \frac{1}{2}\left[\left(\widetilde{h}^{(j)} * c_{j+1}\right)[l] + \left(\widetilde{g}^{(j)} * w_{j+1}\right)[l]\right] \tag{5.2}$$

where $\widetilde{h}$ and $\widetilde{g}$ are the filters corresponding to analysis filter pairs h and g, respectively. The only exact reconstruction condition [91] for the filter bank $(h, g, \widetilde{h}, \widetilde{g})$ is given by,

$$H(z^{-1})\widetilde{H}(z) + G(z^{-1})\widetilde{G}(z) = 1 \tag{5.3}$$

where $H(z)$ is the z-transform of a filter h and so on. This condition determines how one should design the synthesis type filter bank given the analysis filters providing a higher degree of freedom when compared the DWT.

Extension of the à trous algorithm to 2D is straightforward.

$$c_{j+1}[k,l] = \left(\overline{h}^{(j)}\overline{h}^{(j)} * c_j\right)[k,l]$$

$$w^h_{j+1}[k,l] = \left(\overline{g}^{(j)}\overline{h}^{(j)} * c_j\right)[k,l]$$

$$w^v_{j+1}[k,l] = \left(\overline{h}^{(j)}\overline{g}^{(j)} * c_j\right)[k,l]$$

$$w^d_{j+1}[k,l] = \left(\overline{g}^{(j)}\overline{g}^{(j)} * c_j\right)[k,l] \tag{5.4}$$

where $hg*c$ is the convolution of c by the separable filter hg (i.e. convolution first along the columns by h and then convolution along the rows by g). At each scale, three wavelet images, w^h, w^v, w^d each of which has the same size as the original image, representing edges of the original image along horizontal, vertical and diagonal directions.

In [91], it is shown that using non-bi-orthogonal filter banks, one can build the UWT. One example to this is:

$$h^{1D}[k] = [1,4,6,4,1]/16 \quad , k = [-2,..,2]$$
$$h[k,l] = h^{1D}[k]h^{1D}[l] \qquad\qquad (5.5)$$
$$g[k,l] = \delta[k,l] - h[k,l]$$

where δ is defined as $\delta[0,0] = 1$ and $\delta[k,l] = 0$ otherwise. This filter bank is one widely used in analyzing the astronomical data. Following the exact reconstruction condition, it can be shown that for the above analysis filter bank $\tilde{h} = \tilde{g} = \delta$ can be taken as synthesis filters yielding perfect reconstruction. Then just by co-additions of all scales perfectly reconstruct the original image:

$$c_0[k,l] = c_J[k,l] + \sum_{j=1}^{J}\sum_{n=1}^{3} w_j^n[k,l] \qquad\qquad (5.6)$$

where n stands for the three orientations at each scale.

As previously stated, the non-subsampled nature of the decomposition allows one to reconstruct the original image from its wavelet transform in many ways. For a given filter bank (h,g), any filter bank $(\tilde{h}, \tilde{g})$ which satisfies the reconstruction condition given in (5.3), can be used in the reconstruction to obtain the original image. For example, for the analysis filters given in (5.5), $\tilde{h} = h$ and $\tilde{g} = \delta + h$ also constitute the prototype for the synthesis filter bank. For $h=[1\ 4\ 6\ 4\ 1]/16$ corresponding reconstruction filter $\tilde{g} = [1\ 4\ 22\ 4\ 1]/16$ is positive implying it is no longer related to a wavelet function [91].
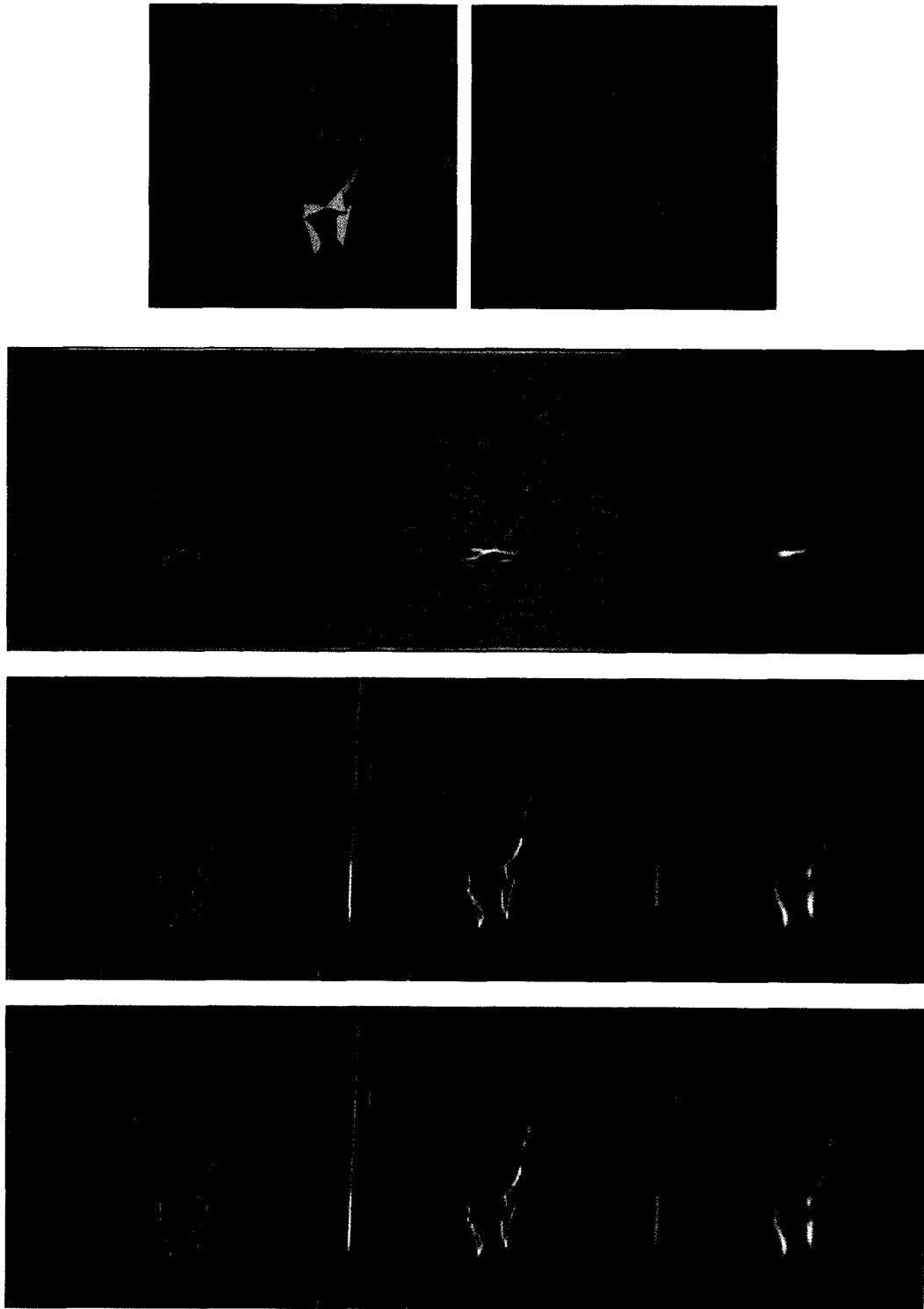
Figure 5.1 Three-level decomposition of *Eintein* image using UWT with the filter bank given in (5.5). Top row: Original and approximation image. 2nd-4th Row: Images of horizontal, vertical and diagonal coefficients each column representing level 1-3 from left to right respectively. Detail images are amplified for the display purpose.

A signal can also be constructed from its Haar wavelet coefficients using the same approach. The Haar filters are h=[0.5 0.5] g=[-0.5 0.5], while the corresponding synthesis filters are determined such that if $\tilde{h}$ =[1 4 6 4 1]/16 is chosen as a smoothing synthesis filter, $\tilde{g}$ = [1,6,16,−6,−1] can be obtained following (5.3). In Figure 5.1 a three-level UWT decomposition of *Einstein* image using the filter bank (5.5) is illustrated to show the capability of the filters in locating the edge features.

5.3 Implementation of the Proposed Algorithm

The first step in the implementation is wavelet domain zero padding (WZP) for an initial estimation of HR image. In WZP the unknown HR image is estimated by zero padding the high-frequency subbands and taking the inverse wavelet transform using the standard DWT. If the LR image in hand is denoted with s of size *mxn*, then the the initial estimate of the HR image is:

$$\hat{x} = IDWT \begin{bmatrix} s & 0_{mxn} \\ 0_{mxn} & 0_{mxn} \end{bmatrix}$$

(5.7)

where 0_{mxn} is the zero matrix of size *mxn* and IDWT is the inverse decimated wavelet transform. In this implementation, the famous JPEG2000 standard CDF 9/7 filterbank is used for taking the inverse transform.

Although the results of the WZP interpolation introduce some blur into the reconstructed image due to low pass nature of the filters used in the inverse transform and lack of the high frequency components, it achieves higher PSNR values over bicubic interpolation and even over the sophisticated method of Carey *et al.* [77,96]. By successful estimation of the high-frequency subband coefficients, it is possible to improve the visual quality of the reconstructed images as well as the PSNR values indicating how close the produced images are to the actual HR images.

The decimated wavelet transform is not shift-invariant and, as a result, non-exact estimation of high-frequency subband coefficients introduces cyclostationarity into the image which manifests itself as ringing in the neighborhood of discontinuities [75]. Celik and Kusetogullari [86] present an interpolation technique using the dual-tree complex wavelet transform (DT-CWT) [87,88] that exhibits approximate shift invariant property and improved directional resolution when compared that of the DWT. In this implementation, the UWT is employed to the WZP-produced HR images in order to provide a good estimation for the detail coefficients in the second step of the proposed technique. The filter bank given in (5.5) is used and one-level decomposition is applied to the WZP processed image to produce the estimated coefficients.

In the third step, the approximation coefficients obtained from the UWT decomposition are replaced with the WZP processed image in a different way to those techniques appear in literature in which the LR image in hand is taken as the low-frequency subband of the DWT. Finally taking the inverse UWT, the estimated final HR image is produced. The scheme of the proposed algorithm is illustrated in Figure 5.2 where UWT^{-1} indicates the inverse undecimated wavelet transform.
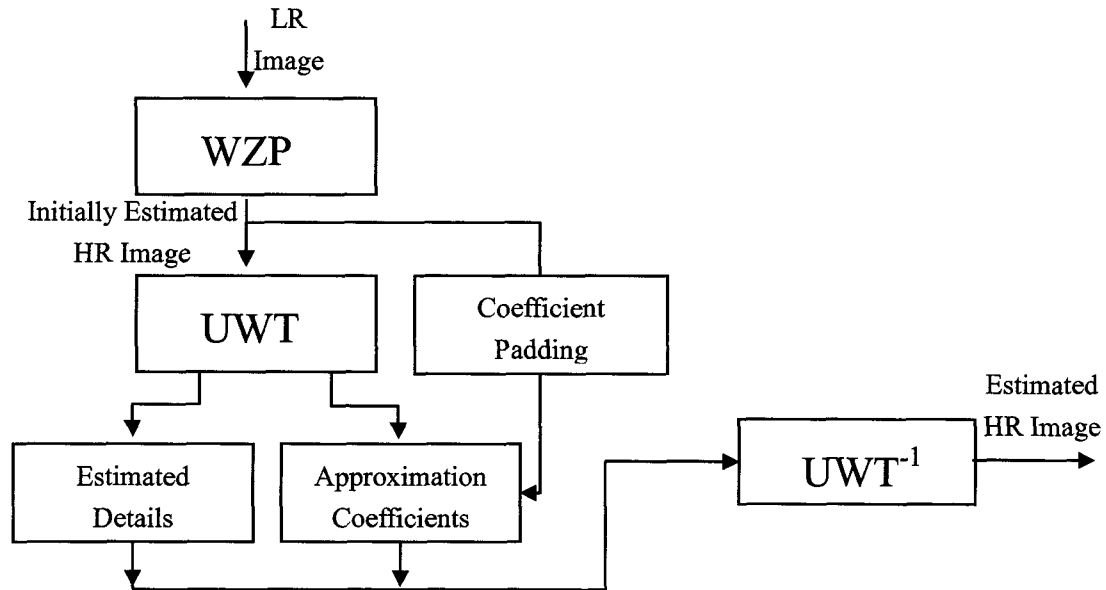
Figure 5.2 The proposed interpolation algorithm.

5.4 Experimental Results and Discussion

5.4.1   Performance Evaluation

In this research's experiments, two different image quality metrics between the original HR images and the reconstructed images from the simulated LR images are utilized to provide objective performance comparisons:

(1) Peak Signal-to-Noise Ratio (PSNR)

(2) Universal Quality Index [97].

PSNR used to show the closeness of the reconstructed image to the original reference image is defined in decibels and given by

$$PSNR = 20\log_{10}\left(\frac{I_{max}}{\varepsilon}\right) \tag{5.8}$$

where I_{max} is equal to 255 for 8-bit images and ε is the root-mean-square (rms) error given by:

$$\varepsilon = \sqrt{\frac{1}{N}\sum (Y(x,y) - X(x,y))^2} \tag{5.9}$$

where $Y(x, y)$ is the original image and $X(x, y)$ is the reconstructed image. N is the number of pixels in the image.

Wang and Bovik [97] propose a universal image quality index (QI) that indicates the similarity between the reference image and the processed one. The QI is defined as:

$$Q = \frac{4\sigma_{xy}\bar{x}\,\bar{y}}{(\sigma_x^2 + \sigma_y^2)(\bar{x}^2 + \bar{y}^2)} \tag{5.10}$$

where $\bar{x}$ and $\bar{y}$ are the mean values while σ_x^2 and σ_y^2 indicate variances of the reference and processed images, respectively and σ_{xy} is the covariance between the two images.

$$\bar{x} = \frac{1}{N} \sum_{i=1}^{N} x_i \qquad , \bar{y} = \frac{1}{N} \sum_{i=1}^{N} y_i \qquad (5.11)$$

$$\sigma_x^2 = \frac{1}{N-1} \sum_{i=1}^{N} (x_i - \bar{x})^2 \qquad , \sigma_y^2 = \frac{1}{N-1} \sum_{i=1}^{N} (y_i - \bar{y})^2 \qquad (5.12)$$

$$\sigma_{xy} = \frac{1}{N-1} \sum_{i=1}^{N} (x_i - \bar{x})(y_i - \bar{y}) \qquad (5.13)$$

where x_i and y_i represent the image pixel values in each image. The range of the Q index is [-1,1] in which 1 is the best value calculated if two images are identical. The quality index constitutes a measure for determining the distortion as a combination of three different factors, i.e. loss of correlation, luminance and contrast distortions. (5.10) is rewritten as a product of three components as:

$$Q = \frac{\sigma_{xy}}{\sigma_x \sigma_y} \cdot \frac{2\bar{x}\bar{y}}{\bar{x}^2 + \bar{y}^2} \cdot \frac{2\sigma_x \sigma_y}{\sigma_x^2 + \sigma_y^2} \qquad (5.14)$$

The correlation between x and y is measured by the first component of (5.14), how close the mean luminance is between x and y is calculated as the second component, and the degree of contrast similarity is determined by the third component.

In addition to the objective quality assessment, the results from the proposed method, along with the other state-of-the-art interpolation techniques are illustrated to show the degree of the visual quality of the proposed method.

5.4.2 Experimental Results

In this research's experiments, six test images of size 512x512 are used and are illustrated in Figure 5.3 to show the capability of the proposed algorithm. These images are chosen for comparison since they are widely used for this purpose in literature because they provide both high and low frequency content simultaneously. The LR images are simulated from the images shown in Figure 5.3 by low-pass filtering with a 3x3 average filter as a point spread function (PSF) of the imaging system and down sampling by 2 along each dimension.

Figure 5.3 Test images:Left-to-right, Top row: Peppers, Bridge, Elaine.
Bottom row: Barbara, Boat; and Lena.

The power of an interpolation algorithms can then determined based on how much the estimated HR image resembles the actual HR image visually by simply showing the interpolation results from the proposed method and statistically using the two metrics introduced in the previous section. Comparisons between the proposed and other techniques are provided, that are two well-known conventional techniques, bilinear and bicubic interpolation, two wavelet domain techniques [75,86] and two state-of-the-art spatial domain edge-based interpolation techniques [69,74] along with the WZP interpolation. The implementation of the benchmark algorithms is as follows.

For bilinear and bicubic interpolations MATLAB® functions are used, [69] and [74] are realized with the MATLAB® codes provided by the authors, and the method in [75] is implemented. WZP is also implemented since it is one of the steps in [75] as well as the proposed algorithm. Some of the published results for [86] are also shown.

As stated previously, WZP is realized with the CDF 9/7 filters. In the second step of the algorithm, i.e. the estimation of the detail coefficients employs the filter bank of (5.5) and the synthesis filters $\tilde{h} = h$ and $\tilde{g} = \delta + h$ for the inverse UWT at the final reconstruction step.

In Figure 5.4 an example of the interpolation result is shown. In the figure the HR and simulated LR *Barbara* images, the result from the proposed algorithm applied to the LR image along with the initial WZP estimated HR image are given to illustrate the impact of the algorithm. Notice how the UWT based detail estimation improves the visual quality of the initially estimated HR image. Local contrast and sharpness of the WZP-processed images are improved after introducing the estimated details while most of distortions in the LR images are removed. However, the aliasing of the high frequency texture of the Barbara's scarf occurred due to the sampling of the data below the Nyquist rate, appears as in the LR image, is still an issue in the reconstructed image. This issue cannot be solved,

unless HR images are reconstructed from multiple LR images; such a process, which is known as superresolution is out of the scope of this dissertation.

Figure 5.4 The result of the interpolation algorithm. Top left: Original image. Top right:Simulated LR image. Bottom left: WZP result. Bottom right: Final reconstructed image

The PSNR values resulting from the various interpolation methods are given in Table 5.1, while the Quality Index comparison is illustrated in Table 5.2. The PSNR and QI values are calculated with excluding the 10 pixels from the borders of the processed images

in order to make a fair comparison, since for the methods of [69] and [74], the codes provided by the authors do not handle the pixels at the border of the images. From both tables it can be inferred that the proposed algorithm outperforms other methods.

Table 5.1 The PSNR(dB) results for various interpolation methods. The LR images are simulated from corresponding HR images using an average filter of size 3x3 and downsampling by 2 in both dimensions.

Test Images	METHODS						
	Bilinear	Bicubic	NEDI [69]	EGI [74]	CS [75]	Method in [86]	Proposed
Peppers	29.83	30.29	32.24	32.54	33.02	33.75	**33.84**
Bridge	24.64	25.07	25.66	25.99	26.58	26.60	**27.46**
Elaine	30.71	31.04	32.23	32.43	32.73	33.00	**33.08**
Barbara	23.92	24.12	24.45	24.61	24.81	25.13	**25.39**
Boat	26.86	27.34	28.50	28.73	29.27	29.80	**30.19**
Lena	29.70	30.22	32.38	32.59	33.29	33.93	**34.39**

Table 5.2 The Quality Index[97] results for the same experiment explained within the caption of Table 5.1.

Test Images	METHODS						
	Bilinear	Bicubic	NEDI [69]	EGI [74]	CS [75]	Method in [86]	Proposed
Peppers	0.6532	0.6766	0.6862	0.6980	0.7187	0.73	**0.7449**
Bridge	0.6637	0.7080	0.7237	0.7455	0.7825	0.79	**0.8439**
Elaine	0.6138	0.6356	0.6418	0.6529	0.6727	0.69	**0.7078**
Barbara	0.6043	0.6335	0.6600	0.6563	0.6811	0.71	**0.7364**
Boat	0.6072	0.6429	0.6609	0.6779	0.7042	0.73	**0.7521**
Lena	0.6793	0.7087	0.7290	0.7419	0.7661	0.79	**0.8071**

In Figure 5.5 and Figure 5.6, the original *Peppers* and *Bridge* images are shown as well as the interpolation results for both images respectively to illustrate the degree of the visual quality of the proposed interpolations. It can be seen from the figures that among all the interpolation results, the closest to the original ones in terms of local contrast and illumination are the the result of the proposed algorithm. Bilinear and bicubic result suffer from blurring. While methods of [69] and [74] both uses edge-based interpolation techniques they provide good interpolations especially along strong edges producing thin edges in the processed images, however they cannot provide sufficient sharpness for the entire texture of the image scene [74]. The main reason for this is, they are both designed assuming the LR image formation is by dirac sampling, in which LR image is obtained by simply downsampling the original image discarding every other pixel along both rows and columns. It seems that it is more realistic to assume a low pass filter as a PSF in the LR image formation. The Cycle Spinning method [75] uses WZP interpolation in its method in such a way that by shifting the WZP-processed image and taking the forward and inverse DWT of it for several distinct shifts to get rid of the ringing artifacts that appear along the strong edges of the WZP-processed images. Therefore, the images produced by this method almost have the same appearance with WZP processed images except for a mild improvement around the edges. The resulting sharpness of the images is not as good as the one produced by the proposed algorithm.

In Figure 5.7, another comparison example is given to illustrate the effectiveness of the proposed method. In the figure, the residual images, i.e. the difference image between the reconstructed image and the ground truth image are shown. Clearly, the proposed algorithm produces the best result when compared to the benchmark methods.

In Figure 5.8, two examples for color image interpolation are shown. The PSNR and QI values are also provided for the comparison. The interpolations are carried out in each color channel separately. Again the highest quantities are produced by the proposed method.
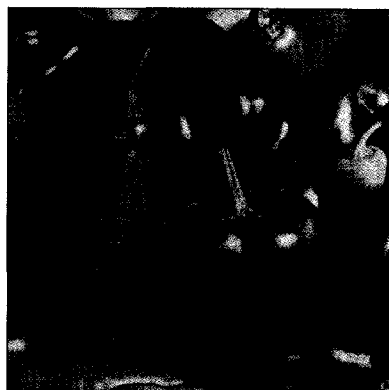
(a) Original
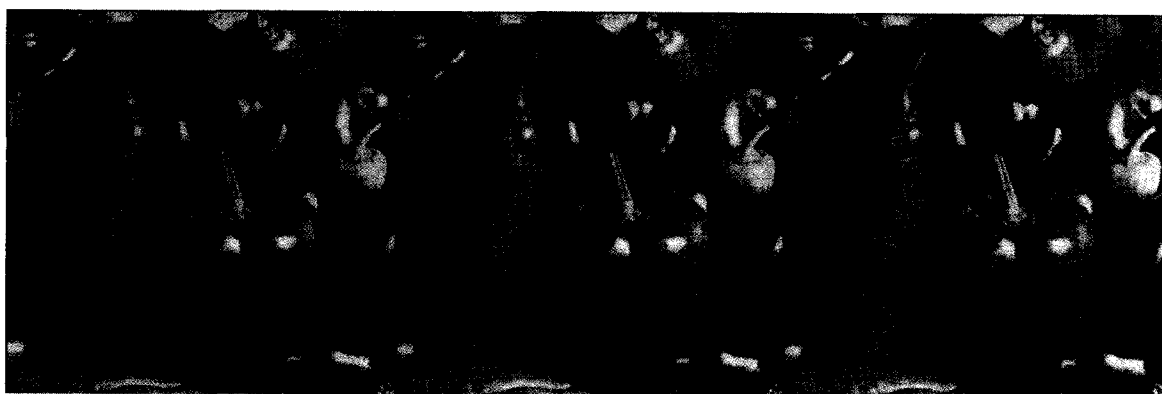
(b) Bilinear **(c)** Bicubic **(d)** NEDI [69]

(e) EGI [74] **(f)** Cycle Spinning [75] **(g)** Proposed

Figure 5.5 Interpolation results of the image *Peppers*.

(a)   Original
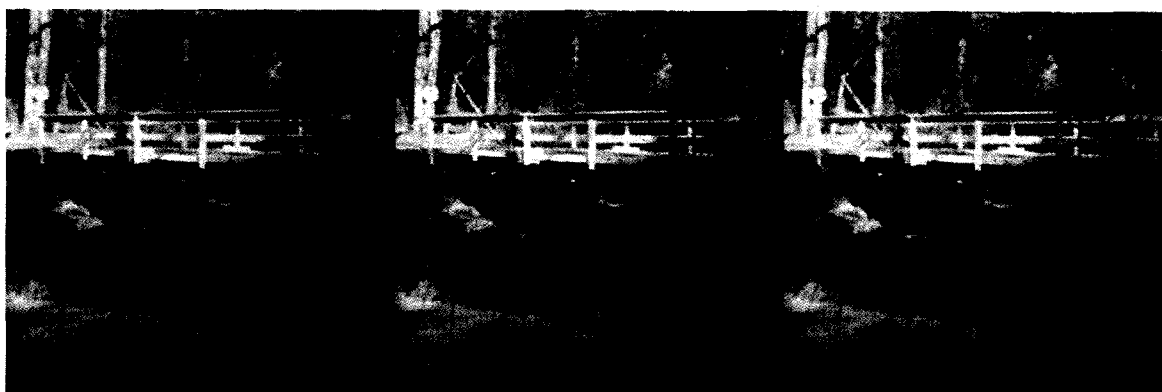
(b)   Bilinear   (c)   Bicubic   (d)   NEDI [69]
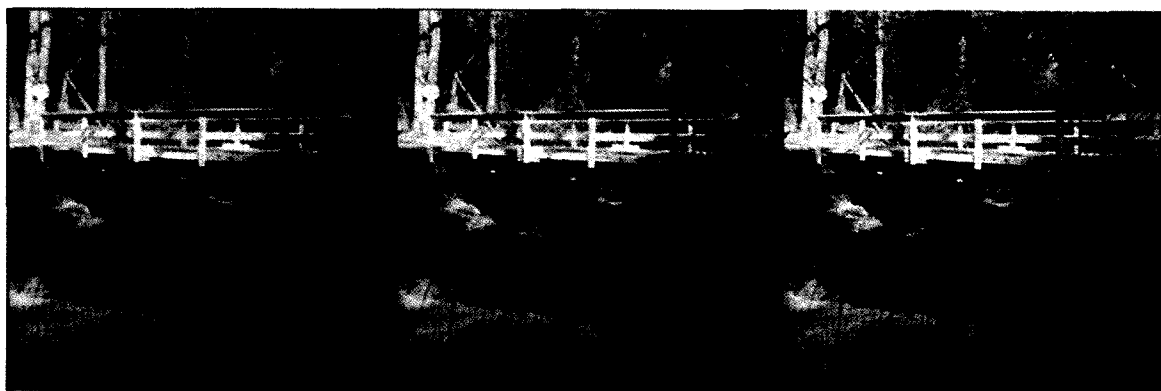
(e)   EGI [74]   (f)   Cycle Spinning [75]   (g) Proposed

Figure 5.6 Interpolation results of the image *Bridge*

(a) Original

(c) Bilinear **(d)** Bicubic **(e)** NEDI [69]

(f) EGI [74] **(g)** Cycle Spinning [75] **(h)** Proposed
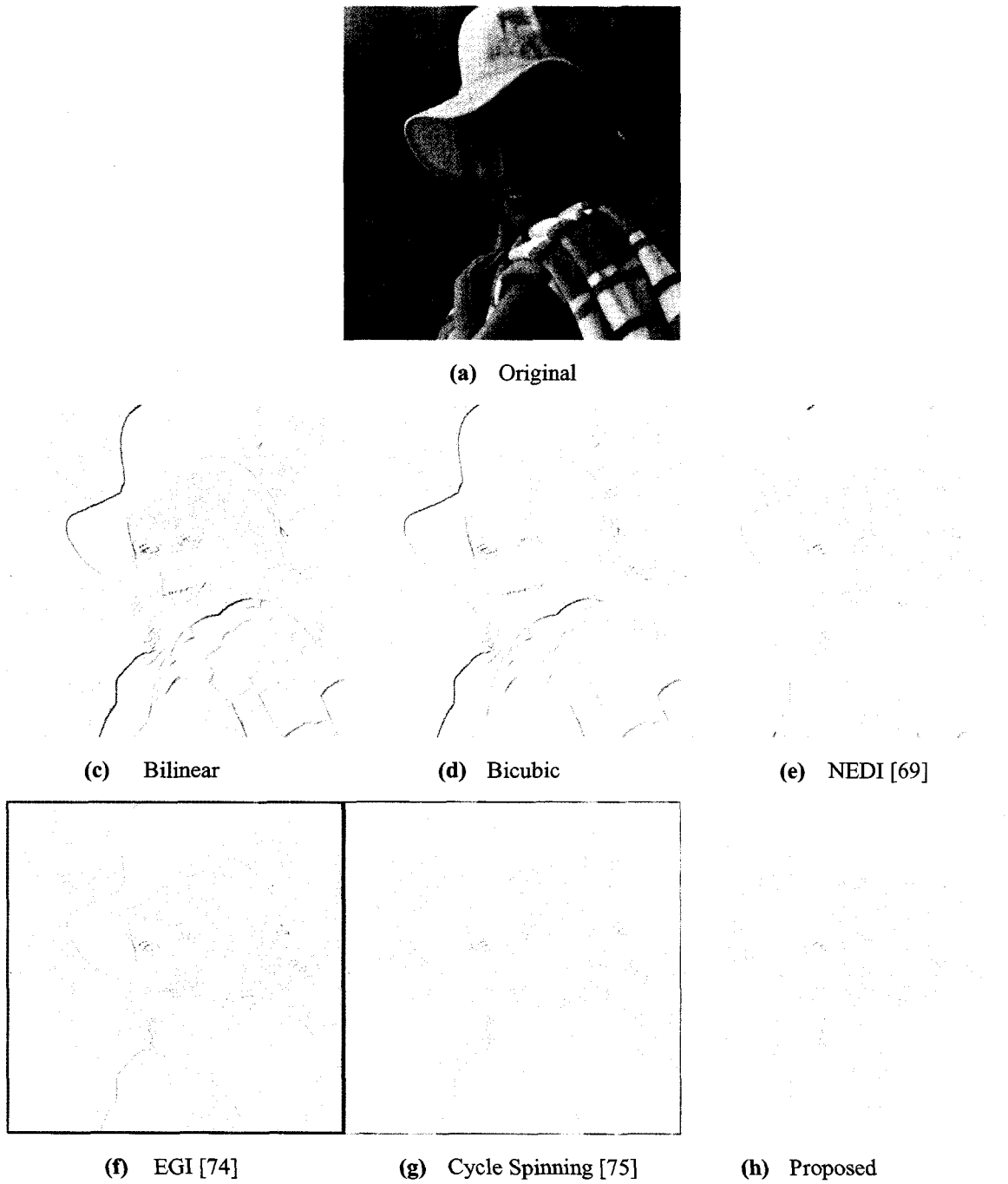
Figure 5.7 Comparison of the residual images between the original *Elaine* image and images reconstructed from LR *Elaine* image.
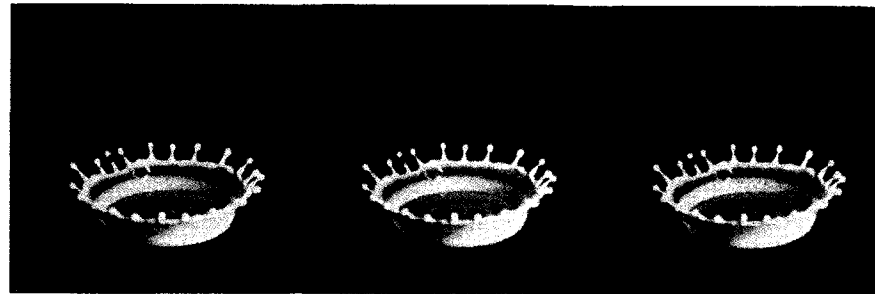
(a1) Original   **(b1)**PSNR:33.38 QI:0.65 **(c1)**PSNR:36.15 QI:0.66
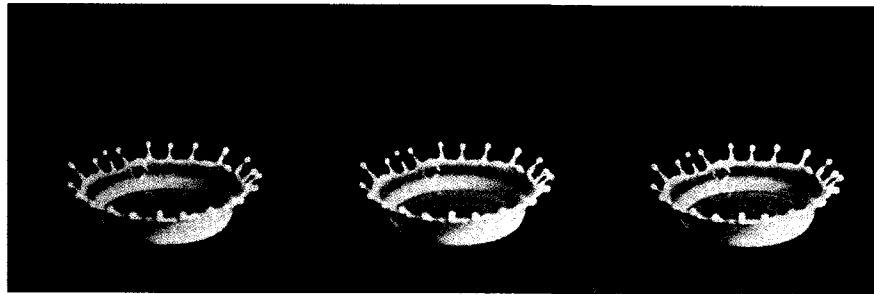
(d1) PSNR:36.55 QI:0.68   **(e1)** PSNR:37.18 QI:0.71 **(f1)** PSNR:38.13 QI:0.76
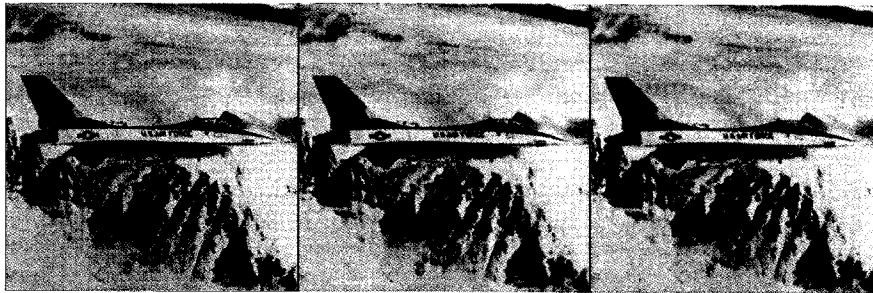
(a2) Original   **(b2)**PSNR:33.38 QI:0.65 **(c2)**PSNR:36.15 QI:0.66

(d2) PSNR:36.55 QI:0.68   **(e2)** PSNR:37.18 QI:0.71 **(f2)** PSNR:38.13 QI:0.76

Figure 5.8: The subjective and quantitative performance comparisons (a) Original images, *Splash* and *F16.*
(b) Bicubic (c) NEDI [69] (d) EGI [74] (e) Cycle Spin [75] (f) Proposed.

Finally, in Figure 5.9 and Figure 5.10, two more image enhancement results are presented to show what will happen if the interpolation method introduced in this Chapter and the WDRC algorithm of Chapters 3-4 are applied together to enhance the feature visibility in images that suffer from poor visibility. The algorithms may be applied sequentially; first the proposed interpolation followed by the WDRC enhancement.

Figure 5.9: The proposed interpolation followed by the proposed enhancement results.
Top left: Original image, top: Interpolated image, bottom: Enhanced image
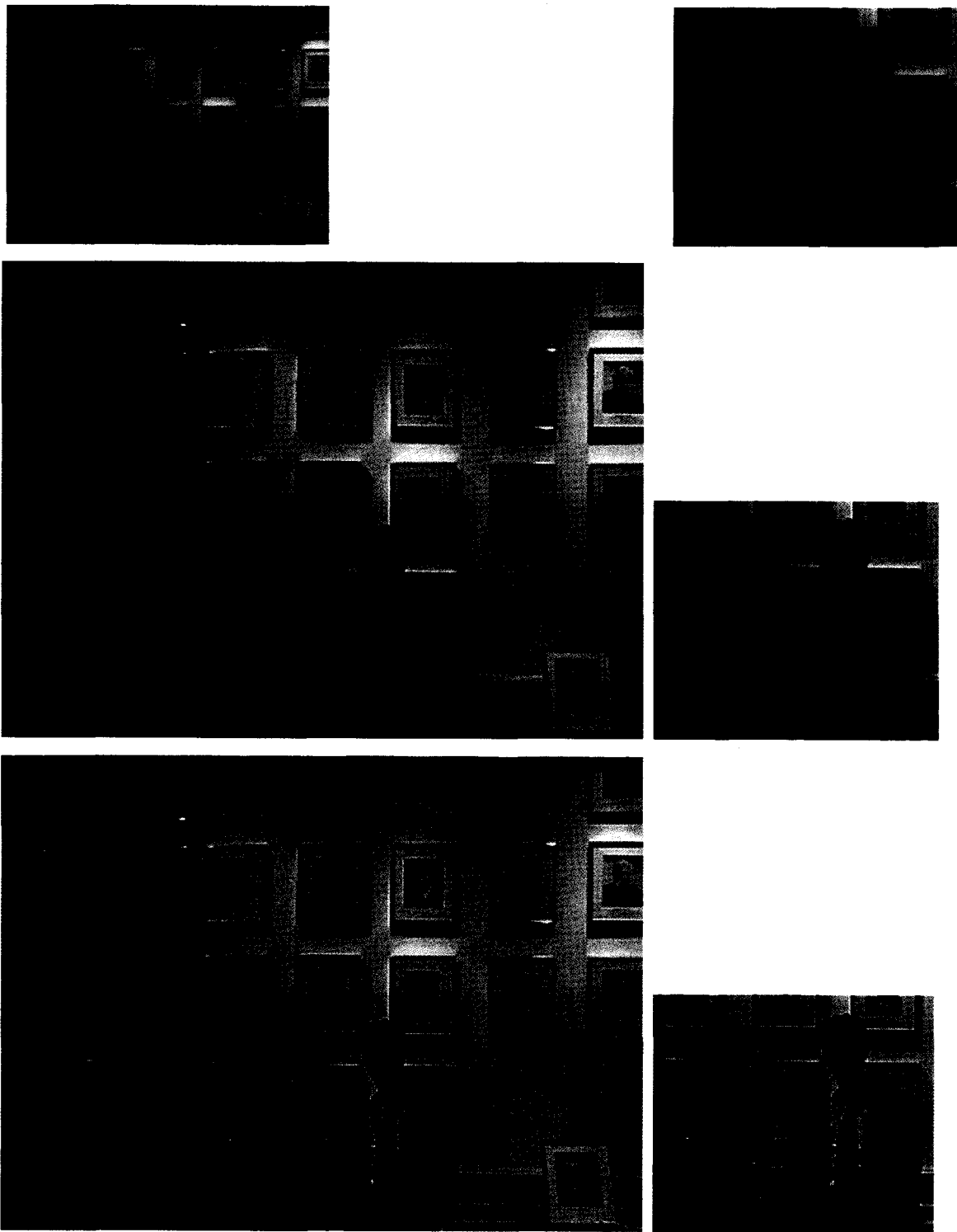
Figure 5.10: The proposed interpolation followed by the proposed enhancement results. Left column top to bottom row: Original, interpolated and enhanced images, respectively. Right column: Magnified portions of the images on the left column.
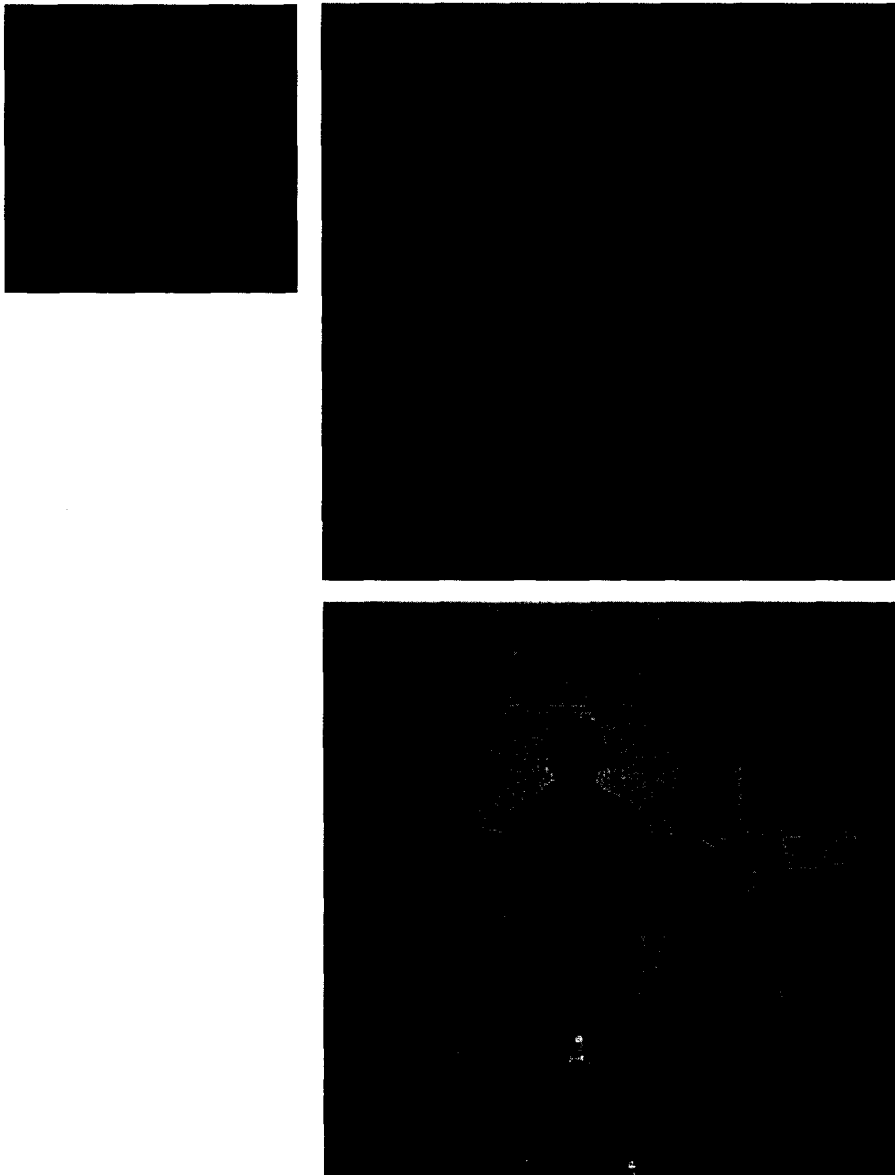
From Figures 5.9 and 5.10, it is obvious that the interpolation when applied with the enhancement algorithms provides a very powerful tool, which can be used in many image processing applications, especially for the ones in which visibility of the image features is crucial.

5.5 Summary of the Chapter.

In this Chapter, a new wavelet-based image interpolation algorithm was introduced for magnifying the image details so that the visibility is improved. The algorithm takes the low resolution image as the low-pass filtered subband of an unknown wavelet transformed high resolution image. Then, an initial high resolution image of size twice the LR image is estimated using zero padding of the details. The HR image is transformed via UWT resulting in four subbands, three of which are related with the high frequency components of the image. In the UWT domain, the LL subband is replaced with the initially estimated HR image and applying the inverse UWT, the final HR image is determined. Experiments conducted with both gray level and color images showed the superiority of the proposed algorithm over the state-of-the-art interpolation methods.

CHAPER VI

CONCLUSIONS AND FUTURE WORK

In this chapter, the major contributions of the dissertation are summarized and possible future work is suggested for further improvement of the proposed algorithms.

6.1 Conclusions

In this dissertation, two wavelet domain image enhancement techniques were developed for visibility improvement of digital images. In the first technique, a general purpose image enhancement algorithm based on the retinex theory has been developed. The second technique deals with the image interpolation problem for visibility improvement of the fine features in the image again in the wavelet domain.

A wavelet-based image enhancement algorithm for dynamic range compression and local contrast enhancement, WDRC, is proposed. The dynamic range compression and the local contrast enhancement are realized on the luminance channel in the transformed domain. The image luminance is enhanced by dynamic range compression of the approximation coefficients successfully using a raised hyperbolic sine curve, then a neighborhood depended contrast enhancement process which utilizes the centre/surround ratio of the Retinex theory is employed to recover the contrast loss occurred due to range compression. The detail coefficients are also modified according to the degree of the enhancement of the approximation coefficients to preserve the edge regularity and finally a linear color restoration process is applied in order to recover the original colors in the image. Experiments have shown that the proposed algorithm provides dynamic range compression, local contrast enhancement, and color rendition simultaneously for a large variety of natural images except for some "pathological" scenes that have very strong

spectral characteristics in a single band such as extremely turbid images. Although the enhanced results are sharper than the original images and the colors of the enhanced results are consistent with the colors in the original images, they are not the colors observed in real-life scenes. This drawback of the proposed algorithm is shared with AINDANE and IRME, as well, since these algorithms, like the proposed one, exploit only the luminance component of the image and restore the colors through a linear process.

In Chapter 4, a new color restoration approach for solving the color constancy issue of the WDRC method is introduced. The color restoration process which maps the ill-conditioned recorded scene illuminant spectral distribution in the original image linearly to the enhanced image, is the main reason for this drawback. For tackling the color constancy problem a novel technique is proposed. The illuminant is modeled as it has an effect on the image histogram as a linear shift and for discounting the effect of the illuminant, a histogram adjustment process is proposed. Following the histogram adjustment process, the WDRC algorithm is applied for dynamic range compression and local contrast enhancement in the luminance channel except for the color restoration. Finally instead of using a linear process of the WDRC, a non-linear color restoration process employing the spectral context relationships of the original image is applied to the enhanced intensity image to produce the enhanced color image. Experiments conducted with numerous images show that the proposed algorithm provides appealing rendition and color constancy better than the state-of-the-art methods. The proposed algorithm is also computationally more effective than other retinex based enhancement techniques.

In this dissertation research, a new wavelet-based image interpolation algorithm was also developed for magnifying the image details so that the visibility of the tiny features is improved. The algorithm takes the LR image as the low-pass filtered subband of an unknown wavelet transformed high resolution image. Then an initial HR image of size

twice the LR image is estimated using zero padding of the details. The HR image is transformed via UWT resulting in four subbands, three of which are related with the high frequency components of the image. In the UWT domain, the LL subband is replaced with the initially estimated HR image and applying the inverse UWT, the final HR image is determined. Experiments conducted with both gray level and color images show the superiority of the proposed algorithm over the state-of-the-art interpolation methods. The interpolation algorithm along with the WDRC-CR can be used to improve the visibility of details in the image.

6.2 Future Work

For improving the proposed algorithms, some complementary work is introduced for future investigation.

The impact of the enhancement algorithm is based on either introducing new high frequency components to the image or improving the existing ones. When the LR image is noisy, the contrast enhancement or an increase in the sharpness will inevitably increase the noise. Although this fact was encountered during experiments with the images taken by a simple commercial camera, the behavior of the proposed enhancement on noisy images for different noise levels has not been thoroughly investigated. It is important to determine this balance for further applications including the impact of the proposed algorithm on segmentation or edge detection in noisy images. Furthermore, an improvement to the WDRC algorithm can be proposed to handle the noisy images suppressing the noise while keeping the local contrast and sharpness high.

Most of the existing interpolation techniques also discard the noise in the original image. However, in practice this is not generally valid because noise will be introduced in the image acquisition process. Denoising the noisy image first followed by the interpolation may be an approach but this may not lead to satisfying results due to some

artifacts (blur, block effects, etc) caused by the denoising process. These artifacts will further be amplified in the interpolation stage. Therefore, a new algorithm that can implement denoising and interpolation simultaneously can also be developed as a further research work.

REFERENCES

[1] H. Kolb, "How the retina works," *American Scientist,* Vol. 91, No. 1, pp. 28-35, 2003.

[2] S. M. Pizer, J. B. Zimmerman, and E. Staab, "Adaptive grey level assignment in CT scan display," *Journal of Computer Assistant Tomography,* vol. 8, pp. 300-305, 1984.

[3] J. B. Zimmerman, S. B. Cousins, K. M. Hartzell, M. E. Frisse, and M. G. Kahn, "A psychophysical comparison of two methods for adaptive histogram equalization," *Journal of Digital Imaging,* vol. 2, pp. 82-91, 1989.

[4] S. M. Pizer and E. P. Amburn, "Adaptive histogram equalization and its variations." *Computer Vision, Graphics, and Image Processing,* vol. 39, pp. 355-368, 1987.

[5] K. Rehm and W. J. Dallas, "Artifact suppression in digital chest radiographs enhanced with adaptive histogram equalization," *Proc. SPIE,* vol. 1092, pp. 220-230, 1989.

[6] Y. Jin, L. M. Fayad, and A. F. Laine, "Contrast enhancement by multiscale adaptive histogram equalization," *Proc. SPIE,* vol. 4478, pp. 206-213, 2001.

[7] P. E. Trahanias and A. N. Venetsanopoulos, "Color image enhancement through 3-D histogram equalization," *Proc. of the 11th IAPR Intl. Conf. on Pattern Recognition, The Hague, Netherlands,* pp. 545-548, 1992.

[8] P. A. Mlsna and J. J. Rodriguez, "A multivariate contrast enhancement technique for multispectral images," *IEEE Trans. on Geoscience and Remote Sensing,* vol. 33, pp. 212-216, 1995.

[9] P. A. Mlsna, Q. Zhang, and J. J. Rodriguez, "3-D histogram modification of color images," *Proc. IEEE Intl. Conf. on Image Processing, Lausanne, Switzerland,* vol. 3: pp.1015-1018, 1996.

[10] Q. Zhang, P. A. Mlsna, and J. J. Rodriguez, "A recursive technique for 3-D histogram enhancement of color images," *Proc. IEEE Southwest Symp. on Image Analysis and Interpretation, San Antonio, TX,* pp. 218-223, 1996.

[11] I. M. Bockstein, "Color equalization method and its application to color image processing," *Journal of the Optical Society of America,* vol 3, pp. 735-737, 1986.

[12] I. Pitas and P. Kiniklis, "Multichannel techniques in color image enhancement and modeling," *IEEE Trans. on Image Processing,* vol. 5, pp. 168-171, 1996.

[13] J.J. Rodriguez and C.C. Yang. "High-resolution histogram-modification of color images," *Graphical Models and Image Processing,* vol. 57, pp. 432-440, 1995.

[14] V. Buzuloiu, M. Ciuc, R.M. Rangayyan, and C. Vertan, "Adaptive-neighborhood histogram equalization of color images," *Journal of Electronic Imaging,* vol. 10, pp. 445, 2001.

[15] E. Land and J. McCann, "Lightness and Retinex theory," *Journal of the Optical Society of America,* vol. 61, pp. 1-11, 1971.

[16] E. Land, "The Retinex theory of color vision," *Scientific American,* vol. 237, pp. 108–128, 1977.

[17] E. Land, "Recent advances in Retinex theory and some implications for cortical computations," *Proc. of the National Academy of Science USA,* vol. 80, pp. 5163-5169, 1983.

[18] E. Land, "Recent advances in Retinex theory," *Vision Research,* vol. 26, pp. 7-21, 1986.

[19] J. McCann, S. McKee, and T. Taylor, "Quantitative studies in Retinex theory, a comparison between theoretical predictions and observer responses to the color mondrian experiments," *Vision Research,* vol. 16, pp. 445-458, 1976.

[20] J. Frankle, and J. McCann, "Method and apparatus for lightness imaging," *US Patent #4,384,336,* 1983.

[21] E. Land, "An alternative technique for the computation of the designator in the retinex theory of color vision," *Proc. of the National Academy of Science USA,* vol. 83, pp. 2078-3080, 1986.

[22] A. Hurlbert, "Formal connections between lightness algorithms", *Journal of the Optical Society of America,* vol. 3, pp. 1684-1693, 1986.

[23] J. McCann, "Lessons learned from mondrians applied to real images and color gamuts," *Proc. IS&T/SID 7th Color Imaging Conf.,* pp. 1-8, 1999.

[24] R. Sobol, "Improving the Retinex algorithm for rendering wide dynamic range photographs," *Proc. SPIE,* vol. 4662, pp. 341–348, 2002.

[25] J. McCann, "Capturing a black cat in shade: The past and present of Retinex color appearance models," *Journal of Electronic Imaging,* vol. 13(1), pp. 28–34, 2004.

[26] A. Rizzi, C. Gatta, and D. Marini, "From Retinex to ACE: Issues in developing a new algorithm for unsupervised color equalization," *Journal of Electronic Imaging,* vol. 13, pp. 75-84, 2004.

[27] E. Provenzi, L. De Carli, A. Rizzi, and D. Marini, "Mathematical definition and analysis of the Retinex algorithm," *Journal of the Optical Society of America,* vol. 22, pp. 2613-2621, 2005.

[28] D. J. Jobson, Z. Rahman, and G. A. Woodell, "Properties and performance of a center/surround Retinex," *IEEE Trans. on Image Processing,* vol. 6, pp. 451-462, 1997.

[29] Z. Rahman, D. Jobson, and G. Woodell, "Multiscale Retinex for color image enhancement," *Proc. of the IEEE Intl. Conf. on Image Processing,* vol. 3, pp. 1003-1006, 1996.

[30] Z. Rahman, D. Jobson, and G. Woodell, "Multiscale Retinex for color rendition and dynamic range compression," *Applications of Digital Image Processing XIX,* Denver, Colorado, pp. 9-17, 1996.

[31] D. Jobson, Z. Rahman, and G. Woodell, "A multi-scale Retinex for bridging the gap between color images and the human observation of scenes," *IEEE Trans. on Image Processing: Special Issue on Color Processing,* vol. 6, pp. 965-976, 1997.

[32] Z. Rahman, G. Woodell, and D. Jobson, "A comparison of the multiscale Retinex with other image enhancement techniques," *Proc. of the IS&T 50th Anniversary Conf.,* IS&T, pp. 426-431, 1997.

[33] Z. Rahman, D. J. Jobson, and G. A. Woodell, "Retinex processing for automatic image enhancement", *Journal of Electronic Imaging,* vol. 13-1, pp. 100-110, 2004.

[34] T. Watanabe, Y. Kuwahara, A. Kojima, and T. Kurosawa, "Improvement of color quality with modified linear multi-scale Retinex," *Proc. of the 15th SPIE Symp. on Electronic Imaging,* Santa Clara, CA, pp. 59-69, 2003.

[35] K. Barnard and B. Funt, "Analysis and improvement of multi-scale Retinex," *IS&T/SID 5th Color Imaging Conf.: Color Science, Systems and Applications,* Scottsdale, Arizona, pp. 221-226, 1997.

[36] K. Barnard, G. Finlayson, and B. Funt, "Color constancy for scenes with varying illumination," *Proc. of the 4th European Conf. on Computer Vision,* vol. 2, pp. 1-15, 1996.

[37] D. Jobson, Z. Rahman, and GA Woodell, "Feature visibility limits in the nonlinear enhancement of turbid images", *Proc. SPIE, vol.* 5108, pp. 24–30, 2003.

[38] http://dragon.larc.nasa.gov/retinex/servo2/ (accessed date: Jan, 2010)

[39] K. Barnard and B. Funt, "Analysis and improvement of multi-scale retinex," *Proc. IS&T/SID Color Imaging Conf.: Color Science, Systems and Applications,* pp. 221-226, 1997.

[40] L. Tao and V. K. Asari, "Modified luminance based MSRCR for fast and efficient Image enhancement," *IEEE International Workshop on Applied Imagery and Pattern Recognition, AIPR-2003,* Washington DC, USA, pp.174-179, 2003.

[41] H. Ngo, L. Tao and K. V. Asari, "Design of an efficient architecture for real-time image enhancement based on a luma-dependent nonlinear approach," *Proc. IEEE Intl. Conf. on Information Technology: Coding and Computing – ITCC'04,* Vol. 1, pp. 656-660, 2004.

[42] L. Tao and K. V. Asari, "An adaptive and integrated neighborhood dependent approach for nonlinear enhancement of color images," *Journal of Electronic Imaging,* Vol. 14, No. 4, ,pp. 1.1-1.14., 2005.

[43] L. Tao, R. C. Tompkins, and K. V. Asari, "An illuminance-reflectance model for nonlinear enhancement of video stream for homeland security applications," *IEEE International Workshop on Applied Imagery and Pattern Recognition, AIPR-2005,* Washington DC, October 19 - 21, 2005.

[44] K. V. Asari, E. Oguslu, and S. Arigela, "Nonlinear enhancement of extremely high contrast images for visibility improvement," *Lecture Notes in Computer Science, Proc. of the 5th Indian Conf. on Computer Vision, Graphics and Image Processing - ICVGIP 2006,* vol.4338, pp. 240-251, 2006.

[45] S. Arigela and K. V. Asari, "An adaptive and nonlinear technique for enhancement of extremely high contrast images," *IEEE Computer Society Proc. of Intl. Workshop on Applied Imagery and Pattern Recognition, AIPR-2006,* Washington DC, pp. 24-29, 2006.

[46] J. Woods and S. O'Neil, "Subband coding of images," *IEEE Trans. Acous. Speech Signal Proc.,* vol. 35, pp. 1278-1288, 1986.

[47] P. Vaidyanathan and P. Hoang, "Lattice structures for optimal design and robust implementation of two-channel perfect reconstruction filter banks," *IEEE Trans. Acous. Speech Signal Proc.*, vol. 36, pp. 81-94, 1988.

[48] P. Burt and E. Adelson, "The Laplacian pyramid as a compact image code," *IEEE Trans. Comm.*, vol. 31, pp. 532-540, 1983.

[49] S. Mallat, "A theory for multiresolution signal decomposition: The wavelet representation," *IEEE Trans. Pattern Recog. and Mach. Intellig.*, vol. 11, pp. 674-693, 1989.

[50] D.L. Donoho, "Denoising by soft thresholding," *IEEE Trans. on Information Theory*, pp. 933-936, 1993.

[51] J. C. Brailean and A. K. Katsaggelos, "Simultaneous recursive displacement estimation and restoration of noisy-blurred image sequences," *IEEE Trans. on Image Processing*, vol. 4, pp. 1236-1251, 1995.

[52] S. G. Chang, Y. Bin, and M. Vetterli, "Spatially adaptive wavelet thresholding with context modeling for image denoising," *IEEE Trans. on Image Processing*, vol. 9, pp. 1532-1546, 2000.

[53] J. M. Shapiro, "Embedded image coding using zero trees of wavelet coefficients," *IEEE Image Proc.*, vol. 41, pp. 3445-3462, 1993.

[54] K. Kinebuchi, D. Muresan, and T. Parks, "Image interpolation using wavelet-based hidden markov trees," in *IEEE Int. Conf. Acoustics, Speech, Signal Processing*, pp. 7-11, 2001.

[55] J. L. Starck, F. Murtagh, E. J. Candes, and D. L. Donoho, "Gray and color image contrast enhancement by the curvelet transform," *IEEE Trans. on Image Processing*, vol. 12, pp. 706-717, 2003.

[56] K. V. Velde, "Multi-scale color image enhancement," *Proc. Intl. Conf. Image Processing*, vol. 3, pp. 584-587, 1999.

[57] L. Chen, C. Chen, and K. Parker, "Adaptive feature enhancement for mammographic images with multi-resolution analysis," *Journal of Electronic Imaging*, pp. 467-478, 1997.

[58] J. Fu, H. Lien, and S. Wong, "Wavelet-based HEQ of gastric sonogram images," *Comp. Med. Imaging and Graph.*, pp. 59-68, 2000.

[59] T. Reeves, and M. Jernigan, "Multiscale-based image enhancement," *Canadian Conf. on Elect. and Comp. Engineering*, pp. 500-505, 1997.

[60] B. Peng, W. Fu, and C. Yang, "Contrast enhancement of radiographs using shift invariant wavelet transform," *Wuhan Uni. J. of Nat. Sciences*, pp. 59-62, 2000.

[61] J. Qin and M. R. El-Sakka "A New Wavelet-based Method for Contrast/Edge Enhancement," *IEEE Proc. Intl. Conf. on Image Processing*, vol. 2, pp. 397-400, 2003.

[62] G. Fan and W. Cham, "Model-Based Edge Reconstruction for Low Bit-Rate Wavelet-Compressed Images," *IEEE Trans. Circ.&Syst. for Vid.Tech.*, vol. 10, no.1, pp. 120-132, 2000.

[63] P. J. Beek, P. J. L. Van, "Edge-Based Image Representation and Coding," *Ph.D. dissert.*, Delft Uni. of Technology, 1995.

[64] K. R. Castleman, *Digital Image Processing,* Prentice-Hall International, Inc. 1996.

[65] M. Unser, A. Aldroubi and M. Eden, "Enlargement or Reduction of Digital Images with Minimum Loss of Information," *IEEE Trans. on Image Processing*, vol. 4, pp. 247-258, 1995.

[66] R. G. Keys, "Cubic convolution interpolation for digital image processing", *IEEE Trans. on Acoustics, Speech, Signal Processing*, ASSP-29, pp. 1153–1160, 1981.

[67] S. Fomel, "Three-dimensional seismic data regularization," *Ph.D. dissert.*, Stanford University, 2000.

[68] K. Jensen and D. Anastassiou, "Subpixel edge localization and the interpolationof still images," *IEEE Trans. on Image Processing*, vol. 4, no. 3, pp. 285–295, 1995.

[69] X. Li and M. T. Orchard, "New edge-directed interpolation," *IEEE Trans. on Image Processing*, vol. 10, no. 10, pp. 1521–1527, 2001.

[70] S. Carrato and L. Tenze, "A high quality image interpolator," *IEEE Signal Processing Letters*, vol. 7, no. 6, pp. 132–135, 2000.

[71] Y. Takahashi and A. Taguchi, "An enlargement method of digital images with the predition of high-frequency components," *Proc. Intl. Conf. Acoustics, Speech, Signal Processing*, vol. 4, pp. 3700–3703, 2002.

[72] D. D. Muresan, "Fast edge directed polynomial interpolation," *Proc. Intl. Conf. Image Processing*, vol. 2, pp. 990–993, 2005.

[73] F. Malgouyres and F. Guichard, "Edge direction preserving image zooming: A mathematical and numerical analysis," *SIAM J. Numer. Anal.*, vol. 39, pp. 1–37, 2001.

[74] L. Zhang and X. Wu, "An edge-guided image interpolation algorithm via directional filtering and data fusion," *IEEE Trans. on Image Processing*, vol. 15, no. 8, pp. 2226–2238, 2006.

[75] A. Temizel and T. Vlachos, "Wavelet domain image resolution enhancement using cycle-spinning", *IEE Electronics Letters*, vol. 41, no. 3, pp. 119-121, 2005.

[76] G. G. Chang, Z. Cvetkovic, M. Vetterli. "Resolution enhancement of image using wavelet transform extrema interpolation," *Proc. ICASSP*, vol. 4, pp. 2379–2383, 1995.

[77] W. K. Carey, D. B. Chuang, S. S. Hemami, "Regularity-preserving image interpolation," *IEEE Trans. on Image Processing*, vol. 8, No. 9, pp. 1293-1297, 1999.

[78] S. G. Mallat and S. Zhong. "Characterization of signals from multiscale edges," *IEEE Trans. on Pattern Analysis and Machine Intelligence*, vol. 14(7), pp. 710–732, 1992.

[79] M. S. Crouse, R. D. Nowak, and R. G. Baraniuk, "Wavelet-based statistical signal processing using hidden markov models," *IEEE Trans. on Signal Processing*, vol. 46, pp. 886-902, 1998

[80] H. Greenspan, C. Anderson, and S. Akber, "Image enhancement by nonlinear extrapolation in frequency space," *IEEE Trans. on Image Processing*, vol. 9, pp. 1035-1047, 2000.

[81] P. Burt and R. Kolczybski, "Enhanced image capture through fusion," *Proc. Intl. Conf. on Computer Vision*, Germany, pp. 173-182, 1993.

[82] N. Nguyen, "Numerical Techniques for Image Superresolution," *Ph.D. dissert.*, Stanford Uni., Stanford, CA, Apr. 2000.

[83] N. Nguyen, P. Milanfar, "An efficient wavelet-based algorithm for image superresolution", *Proc. ICIP'00*, vol.2, pp. 351-354, 2000.

[84] C. Ford and D. M. Etter, "Wavelet basis reconstruction of nonuniformly sampled data", *IEEE Trans. Circ. & Syst.*, vol.45, no.8, pp.1165–1168, 1998.

[85] S. Mitevski and M. Bogdanov, "Application of Multiresolutional Basis Fitting Reconstruction in Image Magnifying", *Proc. 9th Telecomnications Forum*, pp. 565-568, Nov. 2001.

[86] T. Celik and H. Kusetogullari "Self-sampled image resolution enhancement using dual-tree complex wavelet transform", *Proc. EUSIPCO 2009* Glasgow, Scotland, August 2009.

[87] N. G. Kingsbury, "The dual-tree complex wavelet transform: A new technique for shift invariance and directional filters," *IEEE Digital Signal Processing Workshop, DSP 98*, Bryce Canyon, paper no 86, 1998.

[88] N. G. Kingsbury, "The dual-tree complex wavelet transform: a new efficient tool for image restoration and enhancement," *Proc. European Signal Processing Conf., EUSIPCO 98*, Rhodes, pp. 319-322, 1998.

[89] N. G. Kingsbury, "Complex wavelets for shift invariant analysis and filtering of signals," *Appl. and Comp. Harmon. Analy*, vol. 10, pp. 234-253, 2001.

[90] R. Gonzalez and R. Woods, *Digital Image Processing*, Addison-Wesley, USA, 1992.

[91] J. L. Starck, J. Fadili, F. Murtagh, "The undecimated wavelet decomposition and its reconstruction," *IEEE Trans. on Image Processing*, vol. 16(2), pp. 297-309, 2007.

[92] P. Dutilleux, "An implementation of the "algorithme à trous" to compute the wavelet transform," *Proc. Wavelets: Time-Frequency Methods and Phase-Space*, pp. 298-304, 1989.

[93] M. Holschneider, R. K.-Martinet, J. Morlet, and P. Tchamitchian, "A real-time algorithm for signal analysis with the help of the wavelet transform," *Wavelets: Time-Frequency Methods and Phase-Space*. New York: Springer-Verlag, pp. 286–297,1989.

[94] M. J. Shensa, "Discrete wavelet transforms: Wedding the à trous and Mallat algorithms," *IEEE Trans. on Signal Processing*, vol. 40, no. 10, pp. 2464–2482, 1992.

[95] J.-L. Starck, M. Elad, and D. L. Donoho, "Redundant multiscale transforms and their application for morphological component analysis," *Adv. Imaging Electron. Phys.*, vol. 132, pp. 287-348, 2004.

[96] X.Li, "Image resolution enhancement via data-driven parametric models in the wavelet space", *EURASIP Journal on Image and Video Processing,* Vol. 2007, Article ID 41516, 2007.

[97] Z.Wang and A. C. Bovik, "A universal image quality index," *IEEE Signal Processing Letters,* vol. 9(3), pp. 81–84, 2002.

VITA

(By August, 2010)

EDUCATION

B.S. Electronics and Communication Engineering, İstanbul Technical University, Türkiye, Spring 1999.
M.S. Electrical and Electronics Engineering, Dokuz Eylül University, Türkiye, Fall 2005.
Ph.D. Electrical and Computer Engineering, Old Dominion University, US, Summer, 2010.

WORK EXPERIENCE

1999 - 2005 Instructor Officer, TUAF Air Technical School.
2008 - Planning Officer, Instructor, TUAF Academy.

RESEARCH PUBLICATIONS

Conference Proceedings:

1. N. Unaldi, S. Temel, K. V. Asari, and Z. Rahman, "An automatic image enhancement technique for aerial imagery", *Proc. of RAST-2009*, pp. 307-312, 2009.

2. S. Temel, N. Unaldi, F. Ince, "Novel terrain relative lunar positioning system using lunar digital elevation maps", *Proc. of RAST-2009*, pp. 597-602, 2009.

3. N. Unaldi, K. V. Asari, and Z. Rahman, "Fast and robust wavelet-based dynamic range compression and contrast enhancement with color restoration," *Proc. of the SPIE Defense and Security Symposium: Visual Information Processing XVII*, vol. 7341, pp. 278-280, 2009.

4. N. Unaldi, P. Sankaran, K. V. Asari, and Z. Rahman, "Image enhancement for improving face detection under non-uniform lighting conditions," *Proc. of ICIP 2008*, pp. 1332-1335, 2008.

5. N. Unaldi, K. V. Asari, and Z. Rahman, "A fast and robust wavelet-based dynamic range compression and contrast enhancement model," *Proc. of the SPIE Defense and Security Symposium: Visual Information Processing XVII*, vol. 6978, pp. 1-12, 2008.

6. N. Unaldi, S. Arigela, K. V. Asari and Z. Rahman, "A nonlinear technique for the enhancement of extremely high contrast images," *Proc. of the SPIE Defense and Security Symposium: Visual Information Processing XVII*, vol. 6978, pp. 1-11, 2008.

7. N. Unaldi and K. V. Asari, "Local statistics based filtering method for enhancement in super-resolution image reconstruction," *Proc. of the SPIE Symposium on Defense & Security 2007: Visual Information Processing XVI,* vol. 6575, pp. 1-10, 2007.

Published Abstracts:

8. N. Unaldi and K. V. Asari, "Adaptive local contrast enhancement applied to super-resolution image reconstruction," *ODU-NSU-EVMS-VTC Research Exposition Day: Research Expo 2007 - 400 Years of Discovery, Ted Constant Hall, Norfolk, VA, (Poster),* pp. 46, 2007.

Publications under review

9. "Wavelet-Based Bio-Inspired Image Enhancement" submitted to *EURASIP Journal on Advances in Signal Processing.*